MAPPING POTENTIAL SOIL SALINIZATION USING RULE BASED OBJECT-ORIENTED IMAGE ANALYSIS

Jacobus Petrus Stals

Thesis presented in partial fulfilment of the requirements for the degree of Master of Natural Sciences at the University of Stellenbosch.

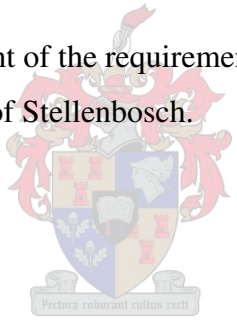

Supervisor: Prof HL Zietsman

DECEMBER 2007

DECLARATION

I, the undersigned, hereby declare that the work contained in this thesis is my own original work and that I have not previously in its entirety or in part submitted it at any university for a degree.

Signature: ----------

Date: ----------

Copyright © 2007 Stellenbosch University
All rights reserved

ABSTRACT

Soil salinization is a world wide environmental problem affecting plant growth and agricultural yields. Remote sensing has been used as a tool to detect and/or manage soil salinity. Object-oriented image analysis is a relatively new image analysis technique which allows analysis at different hierarchical scales, the use of relationships between objects and contextual information in the classification process, and the ability to create a rule based classification procedure. The Lower Orange River in South Africa is a region of successful irrigation farming along the river floodplain but also with the potential risk of soil salinization. This research attempted to detect and map areas of potential high soil salinity using digital aerial photography and digital elevation models.

Image orthorectification was conducted on the digital aerial photographs. The radiometric variances between photographs made radiometric calibration of the photographs necessary. Radiometric calibration on the photographs was conducted using Landsat 7 satellite images as radiometric correction values, and image segmentation as the correction units for the photographs.

After radiometric calibration, object-oriented analysis could be conducted on one analysis region and the developed rule bases applied to the other regions without the need for adjusting parameters. A rule based hierarchical classification was developed to detect vegetation stress from the photographs as well as salinity potential terrain features from the digital elevation models. These rule bases were applied to all analysis blocks.

The detected potential high salinity indicators were analyzed spatially with field collected soil data in order to assess the capability of the classifications to detect actual salinization, as well as to assess which indicators were the best indicators of salinity potential. Vegetation stress was not a good indicator of salinity as many other indicators could also cause vegetation stress. Terrain indicators such as depressions in the landscape at a micro scale were the best indicators of potential soil salinization.

OPSOMMING

Grondversouting is ‘n wêreldwye omgewingsprobleem wat die groei van plante asook landbou opbrengste affekteer. Afstandwaarneming was al gebruik in die opspoor en bestuur van grondversouting. Objek-gerigte beeldanalise is ‘n relatief nuwe beeldanalise tegniek wat analise op verkillende hierargiese vlakke, die verhoudings tussen objekte en kontekstuele informasie in die klassifikasieproses gebruik, asook die vermoë gee om reël gebaseerde klassifikasie prosedures te skep. Die Benede Oranje Rivier in Suid-Afrika is ‘n streek met suksesvolle besproeïngsboerdery op die rivier vloedvlakte, maar is ook blootgestel aan die potensiële risiko van grondversouting. Hierdie navorsing het gepoog om areas van potensiële grondversouting op te spoor en te karteer deur van digitale lugfotografie en digitale elevasie modelle gebruik te maak.

Beeld orto-korreksie is op digitale lugfotos uitgevoer. Radiometriese kalibrasie was nodig a.g.v. die radiometriese verskille tussen foto’s. Radiometriese kalibrasie op die foto’s is onderneem deur Landsat 7 satellietbeelde te gebruik om radiometriese korreksie waardes te bepaal en op korreksie eenhede wat deur middel van beeldsegmentasie verkry is vir die foto’s te gebruik

Na radiometriese kalibrasie kon objek-gerigte analise eers op een analise blok uitgevoer word en die ontwikkelde reël basis op die ander streke toegepas word sonder verstelling van die parameters. ‘n Reël gebaseerde hierargiese klassifikasie is ontwikkel om plantegroei stres vanaf die foto’s asook versoutingspotensiaal terrein eenhede vanaf die digitale elevasie modelle te identifiseer. Hierdie reël basisse is daarna op alle analise blokke toegepas.

Die potensiële versoutingsfaktore is ruimtelik ontleed deur met ingesamelde grond monsters te vergelyk om sodoende die vermoë van die klassifikasies om werklike versouting op te spoor, asook die beste aanwysers van potensiële grondversouting te identifiseer. Plantegroei stress was nie ‘n goeie aanwyser van versouting nie a.g.v. verskeie ander faktore wat ook plantegroei stres kon veroorsaak. Terrein faktore soos

depressies in die landskap, veral op mikro skaal, was goeie aanwysers van potensiële versouting.

ACKNOWLEGEMENTS

My gratitude to the following:

My supervisor, Professor Larry Zietsman, for all the guidance through the thesis.
Mr. Bennie Schloms and Dr. Freddie Ellis for their help.
Theresa Volschenk and Eric Mashimbye at ARC.
The staff at the Department of Geography and Environmental studies for their friendliness and support during my studies.
Wolfgang Lück for his willingness to help and valuable advice.
All my fellow students for making my studies enriching and enjoyable.
My parents for their love and support during this time.
To God my Guide and Strength who made all of this possible through Christ.
To Him the glory!

TABLE OF CONTENTS

DECLARATION ii
ABSTRACT iii
OPSOMMING iv
ACKNOWLEGEMENTS vi
TABLE OF CONTENTS vii
FIGURES ix
TABLES xi
1: INTRODUCTION 1
1.1 Remote sensing in agriculture 2
1.2 Research aims and objectives 3
1.3 Research design 3
1.4 Study area 5
2: SOIL SALINIZATION AND REMOTE SENSING 7
2.1 Soil Salinization 7
2.1.1 Types and extent 7
2.1.2 Definition 8
2.1.3 The causes of soil salinization 8
2.2 Remote Sensing for soil salinity detection 10
2.2.1 Mapping soil salinity 10
2.2.2 Spectral properties of soil and vegetation in salinized areas. 11
2.2.3 Band ratios and vegetation indices 12
2.2.4 Sensor types and transformations 13
2.2.5 Plant indicators of salinity 14
2.2.6 Image classifications 14
2.2.7 Ancillary data 15
2.3 Object-oriented image analysis 15
2.3.1 Image segmentation 16
2.3.2 Rule bases and fuzzy classification 18
2.3.3 Object-oriented landform extraction 20
2.3.4 Vegetation extraction by object-oriented methods 21
3: DATA PREPROCESSING 23
3.1 Available data 23
3.2 Orthorectification 24
3.3 Field boundary delineation 26
3.4 Radiometric Calibration 28

3.5 Mosaicking 31
4: RULE BASE CREATION AND CLASSIFICATION 33
4.1 Classification Strategy 33
4.2 Vegetation Rule Base 34
4.2.1 Vegetation Segmentation 35
4.2.2 Vegetation Class Hierarchy and Classification 38
4.3 Terrain Rule Base 49
4.3.1 Terrain Segmentation 50
4.3.2 Terrain Classification 50
4.4 Automation by Protocols 52
4.5 Image Classification Accuracy Assessment 52
4.5.1 Classification Stability 53
4.5.2 Best Classification Result 54
4.5.3 Accuracy Assessment by Confusion Matrix 54
5: DETERMINATION AND MAPPING OF SALINITY POTENTIAL 57
5.1 accuracy assessment of classifications using ground truth soil samples 57
5.1.1 Soil Samples 57
5.1.2 Determination of salinity potential 58
5.2 Creation of Salinity Potential Maps 68
6: DISCUSSION AND SUMMARY 76
6.1 Vegetation Image Analysis 76
6.2 Terrain Image Analysis 77
6.3 Salinity Detection 77
6.4 Improvements and Recommendations 78
6.5 Summary 79
REFERENCES 80
PERSONAL COMMUNICATIONS 85

FIGURES

Figure 1.1. The research design and workflow. 4
Figure 1.2. The study region within South Africa showing nearby towns. 6
Figure 2.1. The presence of salt on the soil surface in Manitoba, Canada 9
Figure 2.2. The structure of a plant leaf and its electromagnetic response to different wavelengths 11
Figure 2.3. A raw and a segmented image 17
Figure 2.4. Membership functions over a feature range X 19
Figure 2.5. The landform segmentation by Argialas and Tzotsos on a slope dataset and on a DEM combined with ASTER imagery 21
Figure 3.1. The selection of the photos for the mosaics using buffers around soil samples and the photo waypoints 25
Figure 3.2. The filtering and segmentation of the digital images 27
Figure 3.3. An aerial photograph over the Landsat ETM+ image and a segmentation 30
Figure 3.4. A raw (a) and a radiometrically calibrated (b) aerial photograph 31
Figure 3.5. The result of the mosaic process for Analysis Block 2 displaying a 4, 2, 3 band combination. 32
Figure 4.1. Segmentations at 3 different scales 37
Figure 4.2. Membership functions with positive and negative sinusoidal curves and a crisp function 38
Figure 4.3. The rough land cover classification at segmentation level 3 40
Figure 4.4. The feature view was used to find the values of objects in order to define the membership functions of classes 41
Figure 4.5. The problems of varied vineyard appearance 44
Figure 4.6. An example of how samples are chosen for the class BLOCK VEGTATION (green) and BLOCK SOIL (white) 45
Figure 4.7. The Feature Space optimization tool 46
Figure 4.8. The feature view for “relative border to brighter neighbours band (3)” 47
Figure 4.9. The classified field level objects at different segmentation levels 48
Figure 4.10. The DEM, segmentation and classification of the terrain salinity indicators 51

Figure 5.1. The within field vegetation stress mapped by grouping the Z values based on NDVI into five quantiles. 59
Figure 5.2. Buffered zones around soil sample locations and classified salinity indicators. 61
Figure 5.3. The vegetation indicator GRID file clipped with a 50m buffer around a saline and non-saline soil sample. 62
Figure 5.4. Salinity potential map for Analysis Block 1 69
Figure 5.5. Salinity potential map for Analysis Block 2 70
Figure 5.6. Salinity potential map for Analysis Block 3 71
Figure 5.7. Salinity potential map for Analysis Block 4 72
Figure 5.8. Salinity potential map for Analysis Block 5 73
Figure 5.9. Salinity potential map for Analysis Block 6 74

TABLES

Table 3.1. RMS Errors for RGB and NIR photos per block..... 26
Table 4.1. The initial informational classes defined by their pseudo rules..... 35
Table 4.2. The segmentation parameters used in the vegetation rule base classification. 36
Table 4.2. Classification accuracy for the fuzzy classification of agricultural field and vegetation types. 53
Table 4.3. The confusion matrix based on the TTA mask..... 55
Table 5.1. The GRID format classifications clipped by the salinized sample buffers..... 63
Table 5.2. The GRID format classifications clipped by the non-salinized sample buffers 64
Table5.3. The “sum of potentials” field of the saline versus the non-saline buffers aggregated over all analysis blocks..... 65
Table 5.4. The calculation of the salinity potential weights for each indicator based on Tables 5.1 & 5.2. 67

1: INTRODUCTION

Soil is a valuable natural resource making cultivation of crops and subsequent production of food possible. This productive potential can be reduced when land degradation takes place (Stocking 1995). Soil degradation is caused by a change in soil quality brought about by changes in soil properties and processes. Degraded soil can be restored by inputs of fertilizers, chemicals and irrigation. This process is expensive and makes the land dependent on outside inputs to maintain its productivity (Stocking 1995). In this research the environmental problem for which remote sensing detection was applied was soil salinization. Soil salinization is a specific form of land degradation (Szabolcs 1998).

Szabolcs (1998) states that mapping is essential for implementing management practices to prevent salinization. Early identification of salinization is important in combating this problem. The spatial distribution of crops under salt stress can be detected faster and more extensively using remote sensing technologies, than through time consuming and labour intensive ground based inspections (Dehaan & Taylor 2002, Dwivedi et al. 1999).

The Lower Orange River in South Africa is an area of irrigated agriculture producing export quality crops, especially grapes. The project conducted by Volschenk et al. 2005 aimed to determine whether soil salinization in the Lower Orange River occurs due to irrigation practices or from salts washing in from the surrounding terrain. Remote sensing detection of salinization by satellite imagery and digital aerial survey of the irrigated farmland were employed in the study. The results indicated that an improved remote sensing method for identifying salinized irrigated agricultural areas was needed. Object oriented image analysis was proposed by Volschenk et al. (2005).

Leaching of salts in low laying alluvial soils is difficult under waterlogged conditions. The over irrigation of foothills along the Orange River may contribute to the problem of waterlogging as well as the possibility of mobilizing salts that could affect lower laying alluvial soils and thus increasing the potential for soil salinization (Volschenk et al. 2005). This observation is

supported by research from Utset & Borroto (2001) who stated that areas at lower elevation will generally be more saline due to downward lateral flows from irrigated lands at higher elevation.

1.1 REMOTE SENSING IN AGRICULTURE

Remote sensing offers an effective tool for analyzing and mapping environmental phenomena on the earth's surface. Pedologic interpretation is often based on inference rather than direct sensing of the soil qualities. The interpretation of the vegetation cover also holds the key to knowledge of other distributions not directly visible but indirectly through the characteristics and distribution of vegetation cover (Campbell 2002). Finding areas of vegetation stress could be indicative of salinization. Satellite imagery, colour infrared photography and Global Positioning Systems (GPS) can be used to enhance agricultural management by identifying areas with poor soils or monitoring weaknesses in crops (Gibson et al. 2000, Wells & Holz 1985)

Terrain features have also been shown to play an important part in detecting soil salinization. Digital Elevation Models (DEMs) are pixel based models of terrain height and can be used for various forms of topographical analysis. Because of the pixel structure of DEMs, image analysis techniques can also be applied to them.

Using a rule base in Object-Oriented Image Analysis could speed up the process of identifying land cover types and potentially salinized areas and be valuable for future research of this nature (Volschenk et al. 2005). Traditional methods of image classification using per-pixel based methods do not allow the use of spatial parameters in classification whereas object-oriented analysis does (Blaschke & Strobl 2001). In many cases object-oriented classification were equally or more accurate than pixel based methods (Whiteside & Ahmad 2004, Oruc, Marangoz & Buyuksalih 2004, Rego & Koch 2003, Willhauck 2000).

1.2 RESEARCH AIMS AND OBJECTIVES

The aim of the research is to use Object-Oriented Image Analysis techniques to identify and map areas of potential soil salinization along the Lower Orange River.

To achieve this aim the following objectives were set:

- Organize the data and delineate study areas.
- Orthorectify the digital aerial images for the study areas.
- Radiometrically calibrate the digital aerial images in order to reduce radiometric difference between neighbouring images and regions.
- Set up a salinity potential vegetation classification hierarchy using an object-oriented fuzzy classification rule base and execute the classification.
- Set up a salinity potential terrain classification hierarchy using an object oriented-fuzzy classification rule base and execute the classification.
- Do an image classification accuracy assessment of the classified irrigated farmland.
- Record from the classifications of terrain and vegetation the indicators of potentially high salinity by calibrating the potential from existing soil data.
- Map the salinity potentials by summing the weights of all layers of salinity indicators.

The steps to meet the aims and objectives are set out in the research design.

1.3 RESEARCH DESIGN

Figure 1.1 depicts the research design and workflow of the project. There were four main tasks subdivided into smaller subtasks to complete the main task. The main tasks were the Project Setup, Data Preprocessing, Object-Oriented Classification and Verification/Assessment of the results. The four main tasks had to be completed in sequence. Subtasks that had to follow a specific order are indicated with arrows in their order of completion, whereas independent subtasks have no arrows.

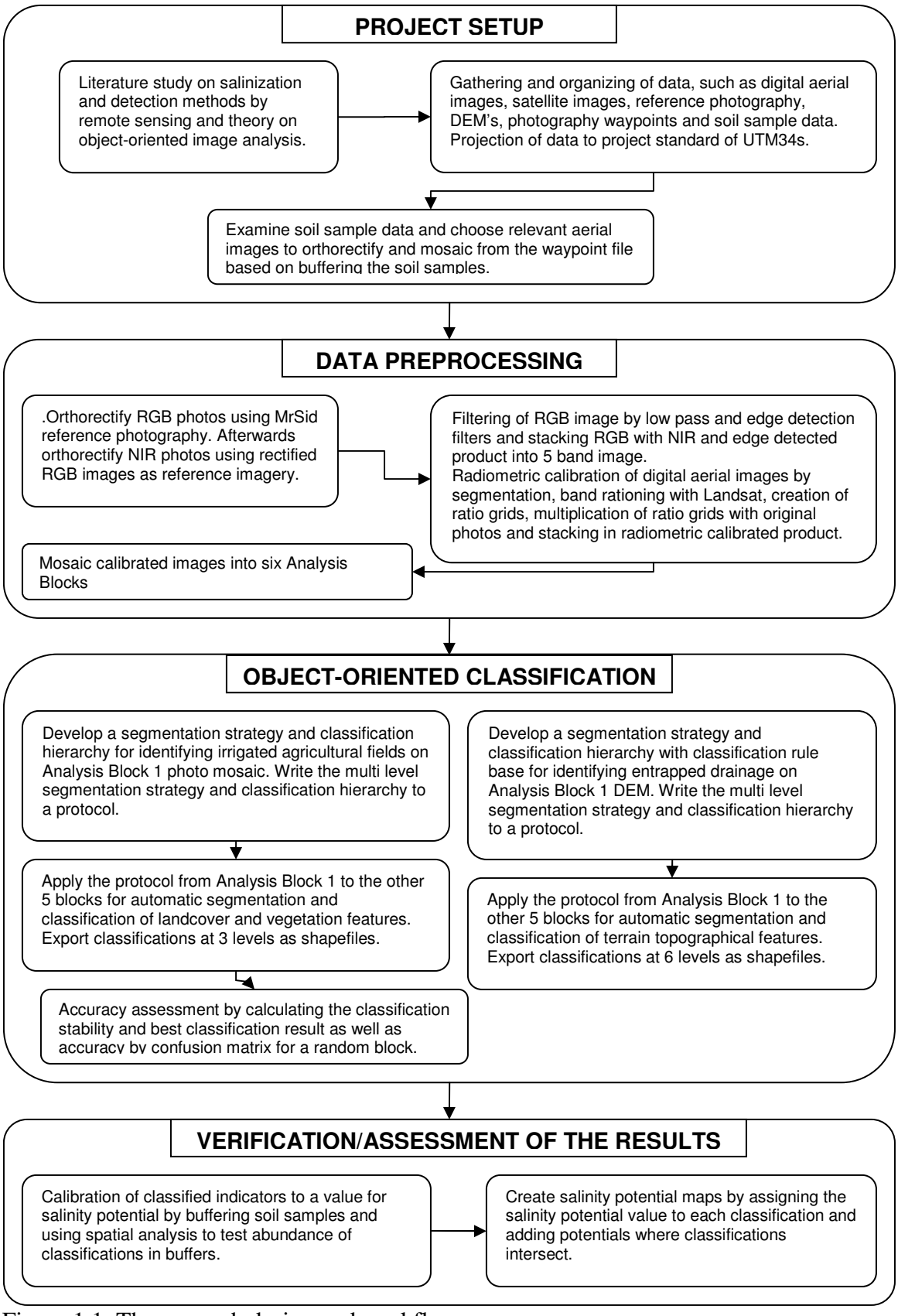

Figure 1.1. The research design and workflow.

The Project Setup phase consisted of researching the literature on the problem under study as well as different image analysis techniques, including an in depth look at object-oriented image analysis as well as gathering and organizing all the raw data that was going to be used. The data for the study was supplied by the Agricultural Research Council (ARC) and the Department of Geography and Environmental Studies at Stellenbosch University from a project done for the Water Research Commission (WRC). Chapter 2 discusses the literature review and Chapter 3 describes the data sources and its organization. The Data Preprocessing stage consisted of processing the raw data into a suitable format for object-oriented image analysis and is covered in Chapter 3. After the data was in a suitable format the creation of rule bases for object-oriented classification could be conducted. Chapter 4 describes the process of rule base creation as well as accuracy assessments conducted on the land cover classification. After classification results were obtained their accuracy in detecting saline land could be verified as well as an assessment made of the salinity potential of the different features that were classified. This process is described in Chapter 5. Maps of potential high salinity were the end products.

1.4 STUDY AREA

The study area stretches roughly from the towns of Upington (upstream) to Augrabies (downstream). See Figure 1.2 for maps of the study area. The Orange River is a westward flowing perennial river (Tooth & McCarthy 2004). The climate in the study region is arid with annual rainfall average of 200mm and a high potential annual evapotranspiration of 2500mm (Water Research Commission, 1999). Granites and gneiss are the common rock types of the sloping terrain bordering the river floodplain along this stretch of the Orange River. The soils on these slopes are minimally weathered, shallow, stony aridisols (Volschenk et al. 2005) while deep alluvial soils are found on the floodplain (Hoffman 1998).

The Lower Orange River has many stretches of irrigated agriculture along its floodplain. This region was the subject of study for the ARC/WRC in a previous project by Volschenk et al. (2005). The majority of the crops under cultivation in the Lower Orange River Water Management Area (WMA) are grapes, cotton, lucerne, wheat and maize (Volschenk et al. 2005).

Figure 1.2 shows the study region for this study consisting of six separate analysis blocks. These analysis blocks were determined from aerial photography that covered the extents of a subset of soil samples from the ARC/WRC project. Image analysis for this study took place in these analysis blocks.

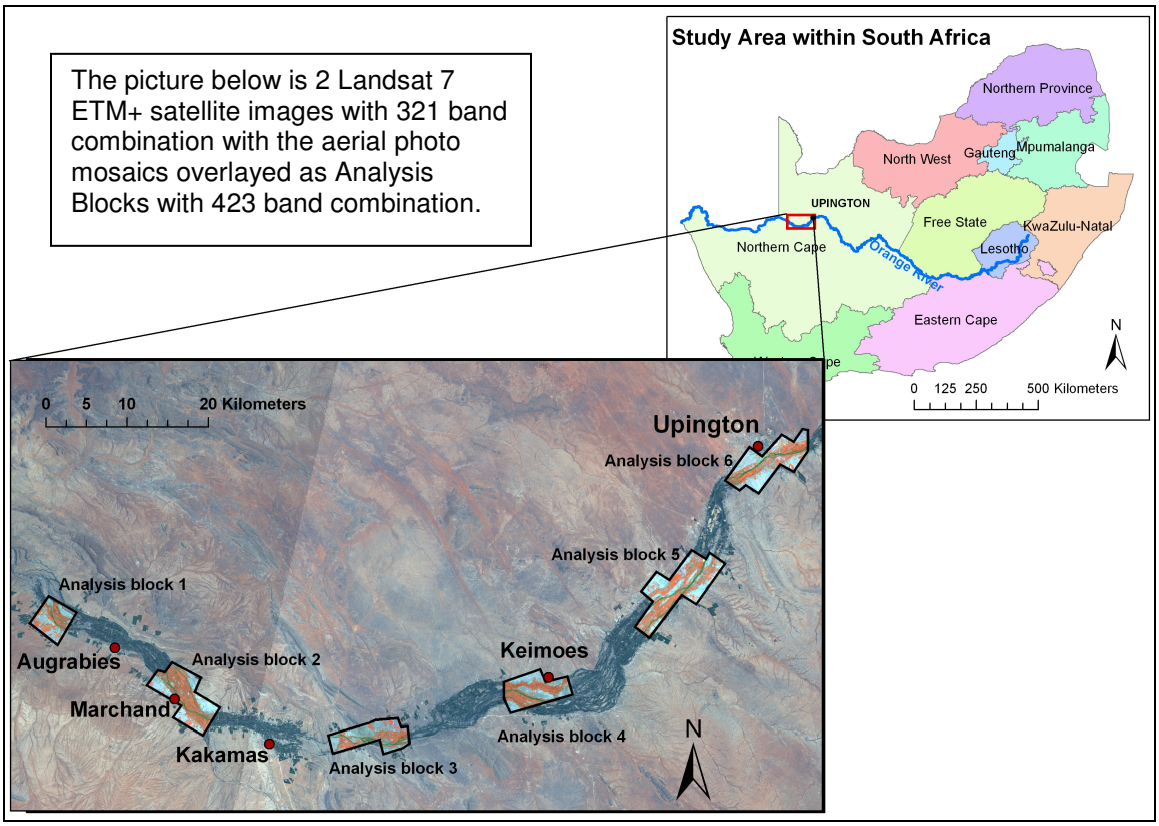

Figure 1.2. The study region within South Africa showing nearby towns.

This chapter defined the aims and objectives of the research and how they were met by the research design that was implemented. A brief description of the study area and the problems of salinization specific to the area was given. The following chapter is a review of the literature on soil salinization, how remote sensing methods have been used to detect it and a brief explanation of object-oriented image analysis.

2: SOIL SALINIZATION AND REMOTE SENSING

Remote sensing methods have been applied extensively for the detection, mapping and prediction of soil salinization. Various forms of spectral, spatial and contextual information as well as different remote sensing and GIS based methods have been applied to this environmental problem faced by land users. Object-oriented image analysis could offer new and unique ways in detecting and managing soil salinity from remote sensing data, and was implemented as analytical method. The phenomenon of soil salinization, the methods used in remote sensing for its detection and modelling, and an extensive background to object-oriented image analysis follows in this chapter.

2.1 SOIL SALINIZATION

This section gives an overview of soil salinization. The types of salinization and the extent worldwide are discussed, followed by a definition of what high soil salinity entails and its effect on plants. Lastly a description of the processes and features that cause high soil salinity is given.

2.1.1 Types and extent

Worldwide two general types of salinization are identified, namely primary and secondary salinization. Primary salinization occurs naturally whereas secondary salinization is caused by human activity (Szabolcs 1998, Peck & Hatton 2003, Barrow 1991, Metternicht 2001). As far as the global extent of high soil salinity is concerned, authors differ in their reports on its extent, but about one billion ha of soil is affected by primary salinization and 77 million ha by secondary salinization of which 58% are situated in irrigated areas. This leads to 20% of irrigated lands worldwide being affected by salinization (Metternicht & Zinck 2003, Ghassemi et al. 1995, Alexandratos 1995).

2.1.2 Definition

The process of soil salinization can be described as the accumulation of water soluble salts such as chlorides, sulfates and carbonates of sodium, magnesium or calcium in the soil profile and soil water at concentrations that limit plant production (Metternicht 2001, McFarlane & Williamson 2002, Steila 1976, Bear 1955, US Salinity Laboratory 1954). Plant production in these conditions becomes limited as the ions in the salts decrease the osmotic potential of the soil water. Thus plants experience physiological drought because they are unable to extract sufficient soil moisture and nutrients and the growth rate is subsequently reduced (Wild 2003, Barrow 1991). Crops without high salt tolerance will show reductions in yield when salts accumulate in the root zone (McFarlane & Williamson 2002). Salinity is commonly measured by electrical conductivity (EC) (Volschenk et al. 2005).

2.1.3 The causes of soil salinization

Primary minerals present in soils and rocks or salts already present in irrigation water serve as the sources of cations and anions present in saline soils (Bresler et al. 1982, US Salinity Laboratory 1954, Bear 1955). The lack of drainage of both subsurface and surface water plays an important part in the process of soil salinization. Soil salinization often occurs in low rainfall arid or semi-arid regions where leaching and transportation of soluble salts is not as effective as in more humid climates (Wild 2003, US Salinity Laboratory 1954, Bresler et al. 1982). Groundwater flow and salinity transport is often linked, especially in semi-arid areas (Peck & Hatton 2003). In these arid conditions water that was in contact with primary minerals, and thus also involved in chemical mineral weathering, act as the transport agent for salts derived from these mineral sources.

Because of the low rainfall in arid and semi arid regions, surface drainage channels are often poorly developed and some drainage may be into drainage basins with little or no exiting stream channels (depressions) (US Salinity Laboratory Staff 1954). These depressions and areas of poor drainage are often associated with soil salinization. Low soil permeability or a high water table

caused by the accumulation of water containing salts in these depressions contribute to salinization. Evaporation of the entrapped surface water in depressions due to low permeability will leave the salts, present in this water, behind on the soil surface and precipitated in the soil profile (Steila 1976, US Salinity Laboratory 1954).

Rising groundwater tables and waterlogging due to entrapped drainage may also encourage the upward movement of saline groundwater to the soil surface or the root zone, and after evaporation salts are precipitated (Wild 2003, US Salinity Laboratory 1954, Bresler et al. 1982). The rising of saline subsoil groundwater tables because of removal of natural vegetation is a cause of soil salinization common in Australia (Pannell & Ewing 2006, Peck & Hatton 2003, McFarlane & Williamson 2002, Kirkby 1996). Soil salinity in irrigated areas may also be caused by human mismanagement in fertilizer application and improper irrigation schemes (Darwish et al. 2005). Figure 2.1 is a photo taken in Manitoba, Canada and illustrates an example of the presence of salts at the soil surface.

Source: University of Manitoba 2006

Figure 2.1. The presence of salt on the soil surface in Manitoba, Canada

As far as irrigation is concerned, irrigation water may also be a source of salinity depending on the quality and source of the irrigation water (Wild 2003, US Salinity Laboratory 1954, Bear 1955). A semi arid to arid climatic region will contribute to high evaporation rates and weaker leaching of salts and drainage of water to the oceans (Bresler et al. 1982, Wild 2003, Steila 1976). The Lower Orange River is situated in a climatic region classified as desert (Tooth & McCarthy 2004), thus arid conditions prevail.

2.2 REMOTE SENSING FOR SOIL SALINITY DETECTION

Metternicht and Zinck (2003) evaluated the constraints as well as some approaches for the use of remote sensing data for salinization detection and monitoring. They state that salts tend to concentrate at the soil surface in increasing levels with increasing soil salinity in dry and irrigated areas, favouring the use of conventional remote sensing tools. Remote sensing technology does however have constraints when the proper nature of salts, the way in which they distribute at the terrain surface and the fast rate of change over time and place of occurrence are considered. The following section describes how remote sensing has been used for salinity detection and monitoring.

2.2.1 Mapping soil salinity

In order to manage current and prevent future salinization, decision-makers and growers need reliable data. Data acquired by monitoring need to first identify places of salinization and secondly detect temporal and spatial changes in salinization (Metternicht & Zinck 2003). Szabolcs (1998) stated that mapping is essential for management practices to prevent salinization. Early identification is important in combating this problem. The spatial distribution of crops under salt stress can be detected faster and more extensively, using remote sensing technologies than through time consuming and labour intensive ground based inspections (Eldiery et al. 2005, Dwivedi et al. 1999, Dehaan & Taylor 2002).

2.2.2 Spectral properties of soil and vegetation in salinized areas.

High salt levels can be detected by remote sensing either as the direct occurrence of salt on the soil surface or indirectly through the vegetation type and growth in a salt affected area (Mougenot, Pouget & Epema 1993 in Metternicht & Zinck 2003). Soil brightness is often associated with soil salinity (Douaoui et al. 2005) with an increase in reflection generally indicating an increase of salt quantity at the terrain surface (Metternicht & Zinck 2003). Severe constraints exist in detecting salinity at the soil surface due to the dynamic nature of the process spectrally, temporally and spatially (Metternicht & Zinck 2003).

Plant response to high salinity levels offers another method of detecting and monitoring salinity. Healthy leaves have a strong reflection in the green part of the electromagnetic spectrum and even a stronger reflection in the near infrared (NIR) band. See Figure 2.2 for an illustration of the structure of a plant leaf.

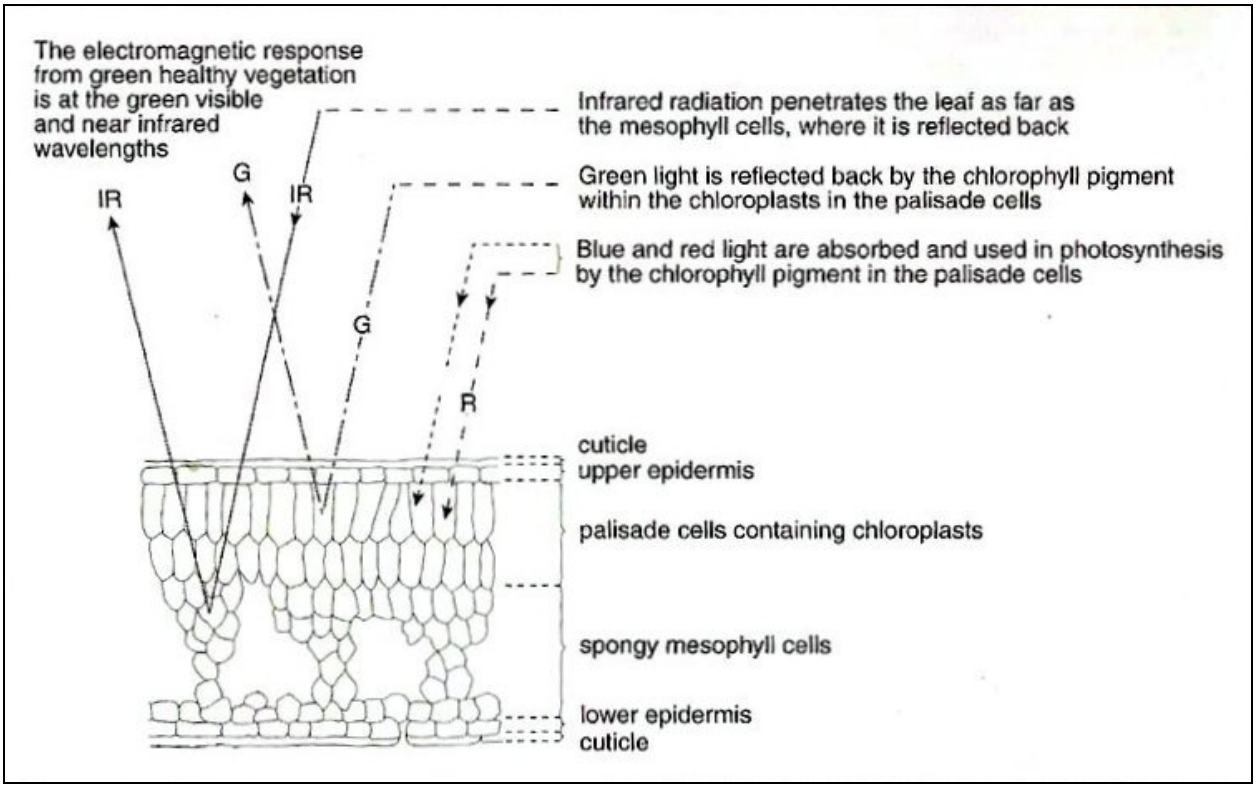

Source: Gibson et al.: 2000

Figure 2.2. The structure of a plant leaf and its electromagnetic response to different wavelengths.

The strong reflection in the NIR band is the result of the mesophyll (spongy tissue) cells in plant leaves. The chlorophyll in the palisade layer of leaves absorb blue and red wavelengths (Gibson et al., 2000). Plant stress results in NIR reflectance reduction and red reflectance increase (Pinter et al 2003). Vegetation indexes such as NDVI can thus be used to examine salt stress in crops (Campbell 2002). Wang et al. (2002) found that the canopy reflectance of soybeans in NIR wavelengths was reduced with increasing soil salinity.

2.2.3 Band ratios and vegetation indices

Many researchers have applied band ratios and vegetation indices for detecting salinization. Some of their findings are referenced in this section. Metternicht & Zinck (2003) found best band selection is necessary for compression of data and securing class separability. Band ratios between visible and near infrared, as well as between infrared bands are better than single bands for identifying salts in soils as well as salt stressed crops. Principal Components Analysis (PCA) could be used for both salt identification and change detection. Pixels of mixed surface features often occur in remote sensing data due to the distribution patterns of salts on the surface. These mixed pixel components can be separated using linear mixture modelling (Metternicht & Zinck 2003).

Eldiery et al. (2005) used multiple regression models to the find best correlation between soil salinity data and corresponding pixel values on satellite image bands. The best model was then used to create salinity maps. Results showed that the green band, near infrared band and the ratio of the near infrared band divided by the red band are strongly related to soil salinity. The selection of the regression model also played an important part in the quality of the salinity map.

Khan et al. (2005) used training areas of salinized land to examine useful spectral bands and band ratios for classifying salinized areas. Salt affected soils were found to have higher reflectance than the other classes. As an indirect measure of salinity in the form of stressed

vegetation, the NDVI was also used. The examined ratios and indices were effective in identifying salinization.

Douaoui et al. (2005) found that vegetation indices showed low correlations with measured salinity values in Algeria. Vegetation cover was not a suitable salinity indicator in that study area. The vegetation indices showed better performance if they were corrected using soil line coefficients. It showed the influence of soil on the spectral response of the surface in the presence of discontinuous vegetation cover.

2.2.4 Sensor types and transformations

The sensor types used for remote sensing based salinity detection found in the review article by Metternicht & Zinck (2003) were aerial photography, airborne videography, infrared thermography, visible and infrared, multispectral and microwave images. The identification of salinity induced plant stress was achieved very well with colour infrared aerial photography. Satellite sensors in the visible to middle infrared range were found in general to obtain good results only when discriminating two surface types, saline from non-saline. Metternicht & Zinck (2003) urges the use of different sensors in improving the accuracy of salinity detection.

Dwivedi & Sreenivas (2002) used multispectral satellite sensors such as Landsat MSS and TM as well as the India Remote Sensing Satellite (IRS-1A) Linear Imaging Selfscanning Sensor (LISS-I). They found the NDVI useful for monitoring vegetation condition. The dynamics of vegetation condition was indicative of the effect of waterlogging and salinization processes. This sensor data have also been used for delineating salinization and/or alkanization (Dwivedi et al. 1999) by visual interpretation methods and also for characterizing salt-affected soils

Airborne remote sensing data have also been used in detecting soil salinization. Dehaan & Taylor (2002) used terrain element classes derived from airborne hyperspectral imagery from the HyMap sensor. These classes were tested against soil sample data in the form of Geonic EM38 (electro magnetic) measurements in a 60m sampling grid in the study area. Health and yield can

be estimated from colour infrared aerial photography, video images and multispectral images using spectral brightness coefficients, photo densities and NDVI (Golovina et al. 1992 in Metternicht & Zinck 2003).

In their review article Metternicht & Zinck (2003) state that various transformations of raw data from satellite sensors allows better discrimination between saline and non-saline classes. Those used include best band selection, Kauth-Thomas transformation, intensity-hue-saturation (IHS) transformation, image differencing, pattern recognition with maximum likelihood classifier, neural networks, decision trees, fuzzy classification and radar backscattering inversion techniques.

2.2.5 Plant indicators of salinity

Halophytic vegetation can act as indicators of the presence of high soil salinity in an undisturbed or natural area (Douaoui et al. 2005, Metternicht & Zinck 2003). The method was not utilized in this study as the natural vegetation in the area was very sparse and irrigated crops were used to detect plant salinity stress. However cotton crops acts as a good indicator of salinity in irrigated drylands because of its health status and yield is correlated to electrical conductivity (Golovina et al. 1992 in Metternicht & Zinck 2003).

2.2.6 Image classifications

Metternicht & Zinck (2003) evaluated some literature on image classification techniques for salinization detection. Fuzzy classification according to fuzzy set theory can avoid misinterpretation of areas of gradual transition between saline and non-saline soils, and have been used as a high accuracy classifier for salt affected areas. Fuzzy logic can provide a good method to classify and monitor environmental conditions related to salinity, and for describing the nature and severity of changes over time (Metternicht 2001). Decision trees and neural networks carry a disadvantage because of their incapability to incorporate prior knowledge about the relationship between input attributes and salinity. A study examined by Metternicht & Zinck

(2003) on radar backscatter inversion techniques found that these techniques were successful in wet conditions.

Mashimbye (2004) found that visual image interpretation, although time consuming, was more successful in identifying salinized irrigated farmland than unsupervised image classification using colour infrared aerial photography.

2.2.7 Ancillary data

Other data not of spectral imagery origin can also be used in combination with remote sensing data in detecting and mapping areas of high soil salinity (Metternicht and Zinck 2003). Based on their previous research Metternicht & Zinck (1996, 1997), encourage the use of data integration in the form of contextual landscape information to improve the spatial discrimination of salinity. They also mention that improvement of salinity monitoring could also be achieved by the use of ancillary data such as topographic, geological and soil maps in combination with satellite imagery, as was done by Sah, Asipit, Murai & Parkpian (1995 in Metternicht and Zinck 2003).

Combining multispectral image data with field data and supporting GIS technology can improve detection accuracy (Metternicht & Zinck 2003). The Land Monitor Project in Australia has mapped the extent of salinity in its western agricultural regions using multi-temporal satellite images and DEMs (Wheaton et al. 1994 in McFarlane & Williamson 2002).

2.3 OBJECT-ORIENTED IMAGE ANALYSIS

Object-oriented image analysis is the remote sensing method used in this study for detecting areas of potential salinization from image and DEM data. A need exists for updating GIS databases with data derived from the increasing amount of good quality Very High Resolution (VHR) imagery. Traditional pixel based classification procedures have often been ineffective to supply data of acceptable accuracy and this paved the way for object-oriented image classification as implemented in eCognition software (Baatz et al. 2004, Schiewe et al. 2001).

The segmentation of an image into image object primitives consisting of one or more pixels forms the basis for object-oriented image classification. These objects contain more than just spectral information, but also information on the shape of the object, spectral texture properties and statistics of pixels within the object and also relations between objects and added thematic layers (Baatz et al. 2004, Hoffmann & Van der Vegt 2001).

A further feature of this method is that various object hierarchical levels with information on relationships between objects at different levels can be stored, as well as relationships to already classified objects on different levels (Baatz et al. 2004). In eCognition a fuzzy knowledge-based classification can be implemented that incorporates spectral, textural, shape, neighbourhood and other types of information into the classification process (Hoffmann & Van der Vegt 2001). Thus the context of an object can also be used in classification (Benz et al. 2004).

2.3.1 Image segmentation

In traditional pixel based methods, classification is conducted by analyzing the image on a pixel by pixel basis instead of objects. Per-pixel classification of VHR imagery reduces the mixed pixel problem but leads to an increase in internal variability and noise within land use classes (Zhang & Maxwell 2006, Schiewe 2002, Schiewe et al. 2001).

Lobo et al. (1996) has used a pre-eCognition segmentation method called IMORM (Iterative Mutually Optimum Region Merging) in classifying landcover and especially separating different crop types. They found that per-segment classification using per-field statistics performed poorly, but that per-segment classification using image derived training samples showed excellent results. They concluded that a method that uses per-segment statistics would probably give the best results.

The first step in object-oriented classification in eCognition is the process of multiresolution image segmentation. The segmentation algorithm segments the image into objects of any chosen

resolution based on their spatial contiguity and spectral properties (Hoffmann & Van der Vegt, 2001). The image objects extracted can be of considerable heterogeneity and therefore act only as information carriers for classification or further segmentation procedures (Baatz et al 2004).

The multiresolution segmentation process starts with single pixel sized objects. In subsequent steps, smaller image objects are merged into bigger objects. Adjacent objects are merged so that their weighted heterogeneity is minimized. This merging process will stop if the smallest growth in defined heterogeneity exceeds the specified scale parameter (Baatz et al 2004). The scale parameter determines the number of objects and sizes in the scene. See Figure 2.3 for a segmentation example. This process follows the hypothesis that segmentation assumes neighbouring image elements to belong to the same class, instead of pixel based methods that consider spectral similarities independently from their occurrence. Homogeneity or heterogeneity parameters will then determine if neighbouring pixels will be included in the region merging (Schiewe et al. 2001)

Figure 2.3. A raw and a segmented image

Other parameters that also need to be entered before segmentation commences is the shape, compactness and smoothness required for objects, as well as weights assigned to each of the spectral bands in the image to be segmented. The weight for the importance of shape homogeneity vs. colour (spectral) homogeneity adds to 1.0 and determines which property takes

priority in segmentation. The shape homogeneity parameter consists of two sub parameters: smoothness and compactness. Smoothness and compactness weights also add to 1.0. High smoothness will attempt to create objects with smooth borders. Compactness is used to differentiate compact objects from non-compact objects with little brightness contrast between the two. The weight entered for these two criteria are not antagonistic, they only indicate which has the highest priority (Baatz et al 2004).

Yuan & Bauer (2006) found the quantitative definition of optimal scale and shape parameters to be a difficult task. Zhang & Maxwell (2006) has also noted that the selection of optimal segmentation parameters for landcover feature extraction with the eCognition approach is a time consuming, trial and error process. Their research proposed a fuzzy logic approach to determine optimal segmentation parameters for effective image segmentation. In this approach an image is first oversegmented (segmented into many small objects) from which object feature values are recorded. These object features serve as input into the fuzzy system to derive the optimal segmentation parameters for the objects desired by the user, which are of larger size.

2.3.2 Rule bases and fuzzy classification

After segmentation, a selected hierarchical level of segmentation can be classified. eCognition uses a fuzzy classification scheme. Fuzzy classification assigns a membership value (usually between 0 and 1.0) to a unit of classification (pixel or in the case of eCognition, an object). Membership functions determine the degree of membership of an object to a class. Objects can have membership values to more than one class (Campbell 1996). In eCognition the class descriptions of each class consists of a set of fuzzy expressions which evaluates specific features of the objects. These expressions can be membership functions, similarities to classes or a nearest neighbour value (Baatz et al 2004). Thus an object may have a membership of 0.8 to forest and 0.3 to water for instance.

The membership functions used in the fuzzy expressions can be either “crisp” resulting in a rectangular function with a definite “yes” or “no” membership to a class, or fuzzy. In Figure 2.4

the blue square indicates a “crisp” set and the red (including the blue square) a fuzzy set over the feature range X_i. The Y axis shows the membership value. The crisp set has only a membership value of 0 or 1.0 over a specified feature range X. The fuzzy set membership value can vary between 0 and 1.0 depending on the feature value.

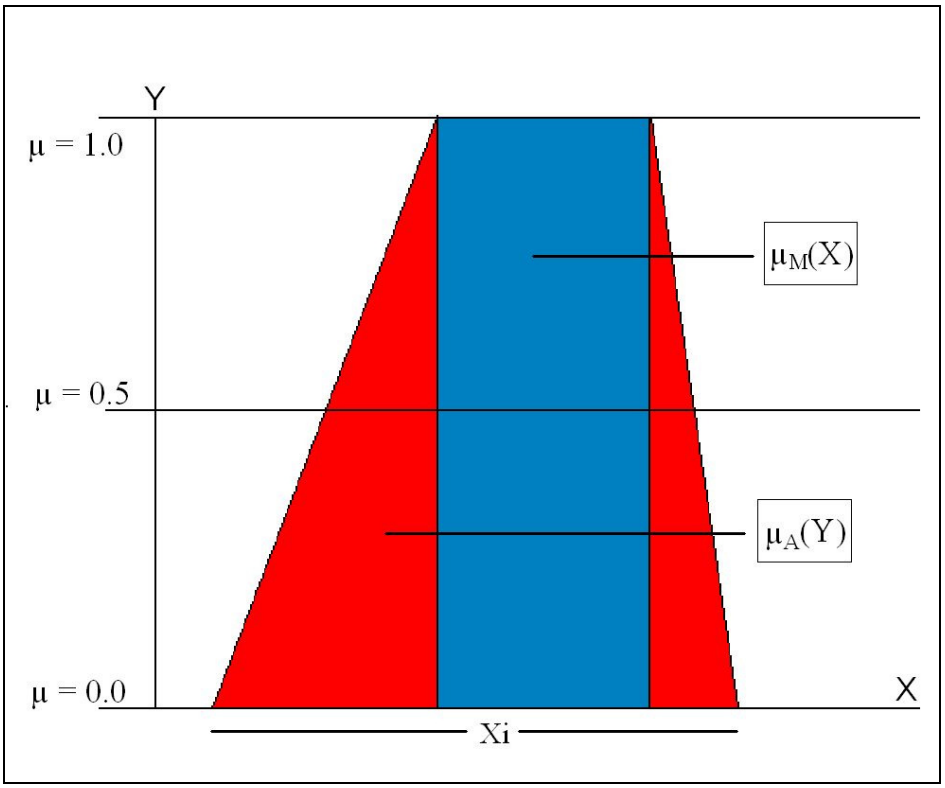

Source: Baatz et al.2004: 70

Figure 2.4. Membership functions over a feature range X

According to the eCognition User Guide (Baatz et al 2004), expert knowledge about the real system being classified can be incorporated into the classification by modelling the membership functions appropriately and thus improving the classification. Fuzzy rule bases consist of a combination of fuzzy rules made up of fuzzy sets. The simplest fuzzy rule is dependant on only one fuzzy set. Fuzzy sets can be combined using operators that return one fuzzy value for all the sets. The operators are “AND” and “OR” with AND returning the minimum value of the sets and OR returning the maximum value of the sets. The final return value of the fuzzy rules then acts as the final degree of membership to the class defined by the fuzzy rule base in the classification. The higher the degree of membership of an object to the class with highest output membership value, the more reliable the assignment is to that class (Baatz et al 2004).

Bauer & Steinnocher (2001) developed a rule base which was incorporated into eCognition for the automatic classification of urban land use areas. The rule base was developed for automating the identification of urban land use classes in high resolution imagery. Historically this process was often executed through time consuming visual interpretation. The morphological properties and spatial patterns of the land cover objects of a pre-classification were first analyzed with the Structural Analysing and Mapping System (SAMS). The derived morphological properties and spatial patterns from SAMS were used to construct the rule base for eCognition classification.

2.3.3 Object-oriented landform extraction

Digital terrain analysis is a well established approach used to extract landforms (Zevenbergen & Thorne 1987) but only recently has object relationships been used. Burnett & Blaschke (2003) used object-oriented image analysis for a multi-scale segmentation and an object-relationship modelling approach for landscape analysis using various combined datasets, including imagery and elevation data. They based their analysis method on Hierarchical Patch Dynamics (HPD) as methodological framework. Some object-relationship modelling characteristics were computed automatically (mean spectral values, spectral homogeneity etc.) while others could be determined through rules created by expert knowledge.

The ability to segment a DEM with eCognition at different levels of scale has also been explored by Blaschke & Strobl (2003). From their research they report that landscape units can now algorithmically be defined based on the morphometric parameters derived from DEM's using object-oriented methods and multi-scale segmentation. This method holds great promise and should be researched further. See Figure 2.5 for an example of a segmentation of topographical and spectral data in combination. Argialas & Tzotsos (2006) used eCognition for multi-scale segmentation and knowledge based fuzzy classification of landform units such as alluvial fans, mountain ranges, piedmonts and basins by combining a DEM and spectral data in the form of ASTER imagery. In Figure 2.5a the segmentation was conducted on a slope dataset and in Figure 2.5b on a DEM combined with an ASTER image.

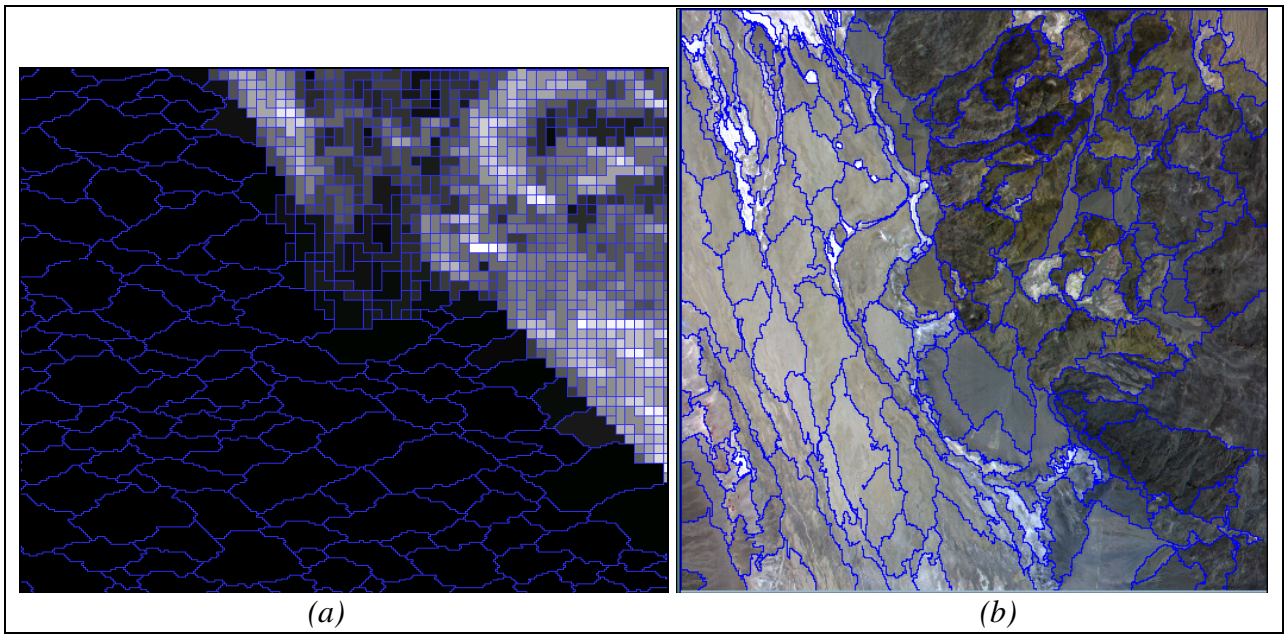

Source: After Argialas & Tzotsos (2006):
Figure 2.5. The landform segmentation by Argialas and Tzotsos on a slope dataset and on a DEM combined with ASTER imagery

2.3.4 Vegetation extraction by object-oriented methods

Chen et al (2005) implemented eCognition segmentation and knowledge based classification on combined LIDAR and aerial photography for differentiating vegetated from non-vegetated areas, for the purpose of tree canopy modelling. Their method included watershed segmentation on the LIDAR height data, limited to the extracted vegetated areas. They managed to model individual trees with a minimum accuracy of 88%.

Brooks et al (2006) used eCognition with sample areas and its Nearest Neighbour classifier to classify different crop types in South-eastern Michigan. The classification results were compared with a pixel based classification. Both methods had similar accuracies (68% for object-oriented and 69.8% for pixel based), but the eCognition classification was found to produce a map that better resembles the rectangular shaped farm fields and is thus visually more pleasing. Urban classes were also much less likely to be assigned to a farm field class. The object-oriented

method produced better accuracies if two dates of Landsat imagery was used instead of a single date image.

This chapter gave a review on the topics of salinization, its detection by remote sensing and other spatially based methods and an explanation of object-oriented image analysis. The following chapter deals with the data for the study and how it was manipulated to prepare it for analysis.

3: DATA PREPROCESSING

Considerable data preprocessing is required before object-oriented image analysis can be conducted in an effective way. The following chapter outlines the data that was acquired and how it was processed in preparation for object-oriented image analysis.

3.1 AVAILABLE DATA

Some of the data available was generated as part of a project funded by the Water Research Commission (WRC) on salinization in the Lower Orange River, South Africa. This data consisted of colour RGB (Red Green Blue) digital aerial photographs as well as near infrared (NIR) digital aerial photographs in TIFF format. The RGB and NIR flights followed the same flight plan and photos were taken to correspond spatially. These photos were taken at an average flying height of 3650m above land surface and each covered a ground area of about 5km x 5km. The camera had a 50mm focal length and 9 micron pixel size with about 4000 rows and columns for each photo image (Volschenk et al. 2005). Unfortunately no calibration report for the camera was available. An ESRI shapefile of waypoints containing the GPS coordinates of all the photos taken was included.

DEM's with 25m spatial resolution created for the WRC project from 5 m contours were acquired from the Department of Geography and Environmental Studies of Stellenbosch University. A point shapefile containing data for soil samples taken to test soil salinity potentials for the WRC funded project in the study region was also acquired from the Geography Department. Orthorectified aerial photographs for the study region in MrSid format at 0.75m pixel resolution were acquired from the Chief Directorate Surveys and Mapping (CDSM) in Mowbray, Cape Town. These photographs served as reference imagery in orthorectification. Two Landsat 7 ETM+ images were also acquired from the Council for Scientific and Industrial Research's (CSIR's) Satellite Applications Centre (SAC). The satellite images were taken at 26 November and 5 December 2002. The RGB and NIR digital aerial images were taken at 24 November, 16 and 19 December 2002. Only photos taken on 24 November were used in the final

study. It was thus important to have dates for satellite imagery and photos close together to avoid seasonal variation of the irrigated crops and vineyards.

The CDSM MrSid orthophotos were mosaicked into 3 large areas using PCI Geomatica 9. Afterwards they were exported to Erdas .img format. The entire study region was situated within the UTM zone 34 South. It was decided to standardize the projections. All the spatial data, except the WRC photos, which still needed to be orthorectified, were reprojected to this projection using ArcGis 9.1.

3.2 ORTHORECTIFICATION

Orthorectification of the RGB and NIR photos were conducted using Leica Photogrammetry Suite v8.7. To select the photos for orthorectification the point shapefile of soil samples which overlapped the available reference imagery were buffered with 1.5km. The result was a grouping of six areas where soil samples were taken in close proximity. These areas are henceforth called Analysis Blocks. Figure 3.1 illustrates the buffers around soil samples (green points in the figure) and how the photos were selected by waypoints (the red and blue points in the figure). The waypoints (representing the photos) falling within these buffer polygons (points in red in the figure) were to be orthorectified. In some instances unnecessary photos were left out. At a later stage more photos were added to some Analysis Blocks in order to create a spatially complete mosaic. Subsets of the MrSid orthophoto mosaics were made for each Analysis Block as reference imagery.

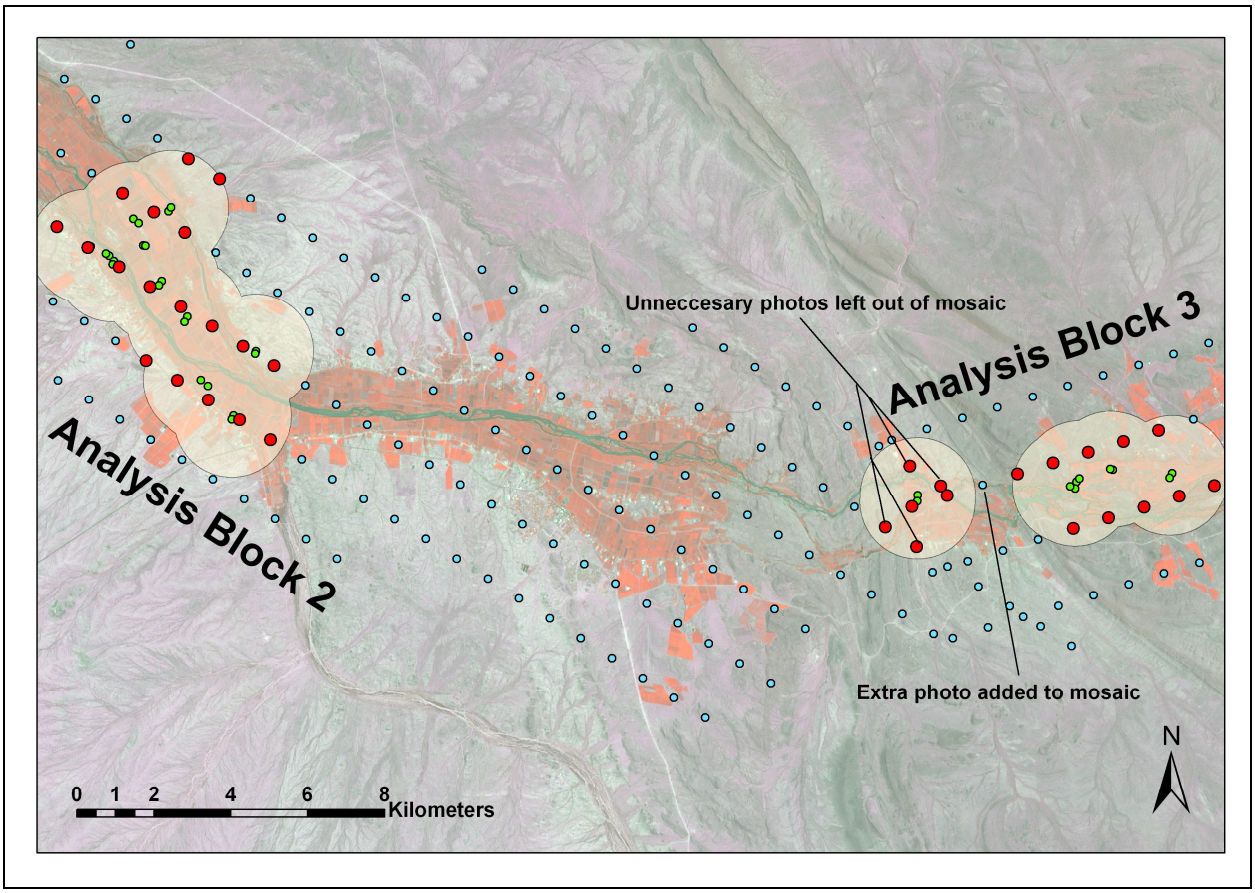

Figure 3.1. The selection of the photos for the mosaics using buffers around soil samples and the photo waypoints

Orthorectification in Leica Photogrammetry Suite (LPS) was done as a separate block project for each Analysis Block and separately for RGB and NIR. The X Y coordinates and Z (height in feet, converted to meters) of the camera were included in the waypoint file for each photo and entered as parameters in the rectification process. Interior and exterior camera orientations were computed automatically by the software using Self Calibrating Bundle Adjustment (SCBA). Ground Control Points (GCPs) and Tie Points were collected using the 25m DEMs as reference height data for orthorectification. Block triangulations were computed and adjustments for the exterior orientation parameters based on the errors computed by the SCBA were entered for subsequent triangulations. This iterative process continued until the errors computed by SCBA were satisfactorily low. The Root Mean Square (RMS) errors achieved for each block are shown in Figure 3.2. Blocks 2 and 4 had very weak RMS errors, but none better were calculated. The NIR RMS errors were better than the RGB errors, probably because the rectified RGB images were used as reference images in collecting GCP's for the NIR orthorectification.

Table 3.1. RMS Errors for RGB and NIR photos per block

Block	RMS X	RMS Y	RMS Z
RGB			
1	1.2257	1.3035	0.8656
2	4.3711	2.8928	5.0604
3	0.7718	0.9577	0.4609
4	2.3073	1.6491	2.4846
5	0.7596	0.7797	1.1785
6	0.8082	0.8774	0.6073
NIR			
1	0.482	0.4924	0.0706
2	2.1575	1.6885	0.2998
3	0.3635	0.4759	0.3407
4	0.3872	0.3239	0.0188
5	0.2996	0.5992	0.1452
6	0.3132	0.4436	0.0121

After satisfactory RMS errors were achieved (less than 1.0 was considered satisfactory) the RGB and NIR photos were orthorectified and resampled using the nearest neighbour method with 0.75m pixel resolution and projected to UTM zone 34 South. The third band of the NIR aerial images was selected to be stacked onto the corresponding RGB image as a fourth band using the image stack command in Erdas Imagine v8.7. Note that in the stacking process the blue band was stacked as band 1 and the red band as band 3 to correspond with the Landsat 7 configuration.

3.3 FIELD BOUNDARY DELINEATION

In order to optimize the eCognition segmentation of individual agricultural field blocks into single objects a suggestion by Lück (2006, pers com) was followed. It entailed running filters over the photo images. Edge detection of field boundaries through filtering might improve segmentation of individual field blocks. Accurate detection of field boundaries was needed to separate irrigated agricultural land from natural surroundings. Only the irrigated farmland was to undergo analysis for vegetation stress as it was not feasible to attempt stress detection on the natural vegetation.

Figure 3.2 illustrates an example of the filtering process and a segmentation result based on the use of the edge detected product in conjunction with the spectral bands (1-4). Figure 3.2a is a photo in the unfiltered state. After examining and testing the available filters, it was decided to use a low pass 7x7 filter for all RGB photos. The purpose was to eliminate the high contrast

between vegetated vineyard rows and bright soil in between the rows for the edge detection to follow (result in Figure 32.b). Next a Prewitt edge detection filter was run on these low pass products. The aim of these filters was to eliminate within field block contrast and to highlight the edges of field blocks. The end result was a 3 band image showing the detected edges of areas of spectral contrast (Figure 3.2c). This edge detected product helped to better segment along individual field block borders and avoid cutting fields in half with segmentation. The second band of the edge detected product was selected and stacked together with the RGB and NIR 4 band image to form a new 5 band image. Figure 3.2d shows a segmentation result on the 5 band image.

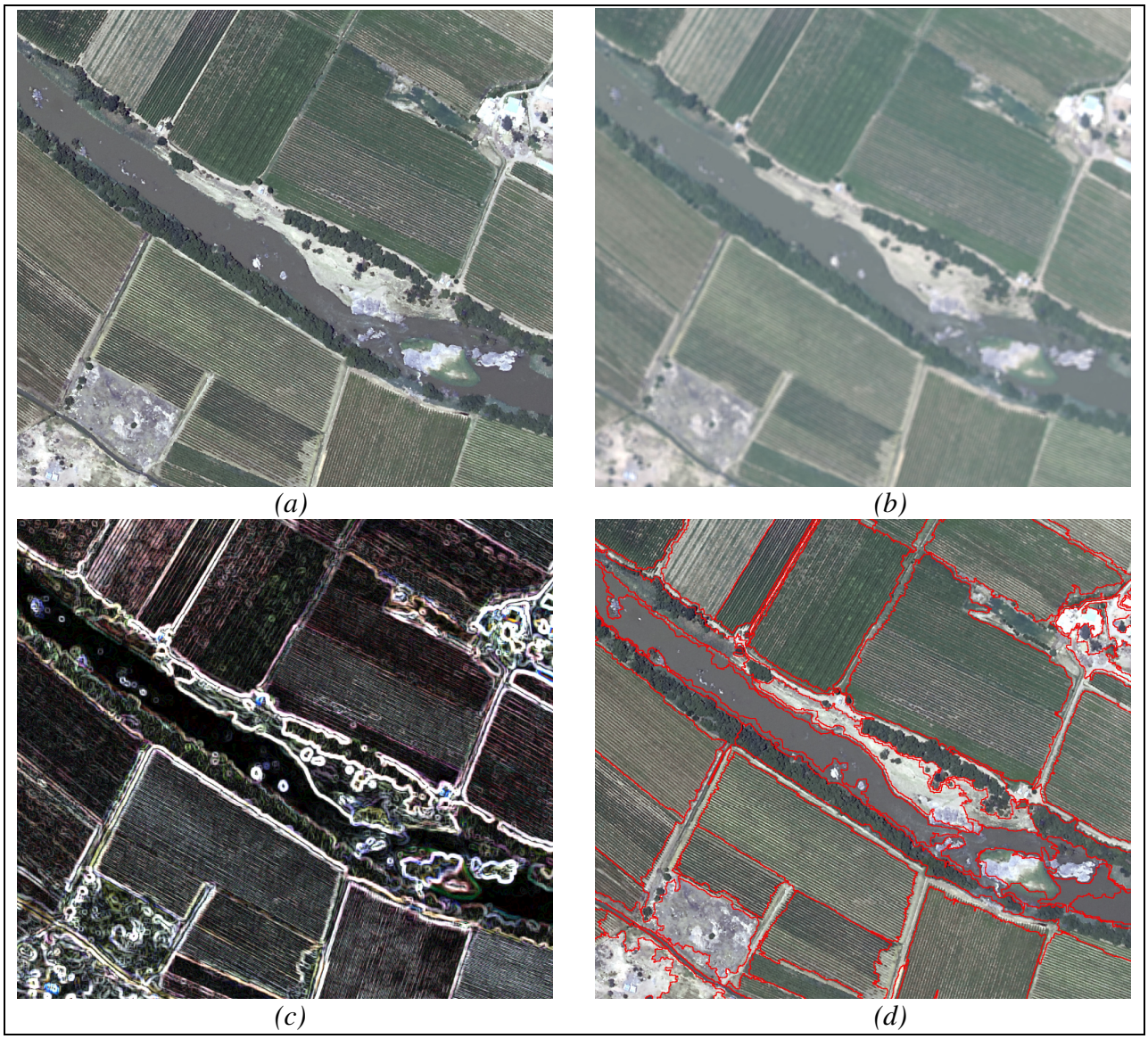

Figure 3.2. The filtering and segmentation of the digital images

3.4 RADIOMETRIC CALIBRATION

Although preprocessing of data alters the original image values and may have unwanted effects on the digital values and thus affect classifications (Campbell 2002), it was deemed necessary to perform extensive radiometric calibration on the aerial images. The WRC Report (Volschenk et al. 2005) stated that radiometric calibration was necessary on the photographs. The report pointed out that an attempt was made to transfer an eCognition rule base developed on one uncalibrated block to another, but that the rule-base parameters needed to be adjusted for the new block of photos thereby loosing any potential advantage of automated feature extraction offered by using a rule based method. Illumination differences between photos and between Analysis Blocks were identified as the cause of the problem (Volschenk et al. 2005). Mashimbye (2004), referring to the RGB and NIR images noted that the lack of radiometric calibration of the digital aerial images results in similar objects showing different reflectance properties, which affects digital image analysis. Mashimbye (2004) deemed it advisable to perform radiometric calibration on the photos before any rule based classification. Upon inspection of the raw photographs, brightness differences were found between the overlapping areas of adjacent photos. Dark patches also occurred on some photographs, assumed to be shadows cast by light clouds.

In the article by Tuominen & Pekkarinen (2004) a method for radiometric calibration of aerial photographs was presented. They stated that bidirectional reflectance causes spectral characteristics of objects to depend on where they are located in the image, therefore similar objects, such as forest stands, will have different characteristics in different locations in the image. (Tuominen & Pekkarinen 2004). They propose a correction method using a satellite image, which is less affected by bidirectional reflectance, for the local adjustment of pixel values of aerial photographs. The general level of brightness of the correction units are determined by the satellite imagery. They used image segmentation on the photographs to create correction units. Using image segmentation to differentiate between land cover classes avoids the problem of correction units containing different land cover types and thus having spectrally different satellite image pixels (Tuominen & Pekkarinen 2004).

The following equation (1) from Tuominen & Pekkarinen (2004) displays the correction for each channel (band) of the aerial image. The same function is applied to different correction unit segments.

$$\hat{E}_{\mathrm{ch_i}}(x,y) = \frac{\overline{E}_{TM_i}}{\overline{E}_{ch_i}} E_{ch_i}(x,y), \qquad (x,y) \in I, i = 1,...,n \qquad (1)$$

$\hat{E}_{\mathrm{ch_i}}(x,y)$ = adjusted value of pixel *(x,y)* of channel *i* of the aerial photograph *I*, *n* is the number of channels, $\bar{E}_{\mathrm{ch}i}$ is the mean of aerial photograph pixel values in the correction unit and $\bar{E}_{\mathrm{TM}i}$ is the mean pixel value of the satellite image band *i* in the correction unit and $E_{ch_i}(x,y)$ is the individual pixel value in the original aerial photo.

As two satellite images of different dates were used for radiometric calibration, it was needed to convert the digital numbers (DN's) to reflectance values and thus have standardized spectral values for the images. The acquired Landsat images were converted from Digital Number (DN) to reflectance values, reflectance rescaled to 8 bit values and the images pan-sharpened to 15m.

Equation (1) was implemented for the first 4 bands, leaving out the edge detection band, in the following steps. The 5 band digital aerial images (consisting of RGB, NIR and the edge detected band) were segmented in eCognition at the same parameters for level 4 (see Chapter 4). The Customise Features tool in eCognition was used to create a ratio feature. This ratio feature divided the Landsat band mean by the corresponding aerial photo band mean per segment for the first four bands (RGB and NIR), satisfying $\frac{\overline{E}_{TM_i}}{\overline{E}_{ch_i}}$ in equation (1). Figure 3.3 illustrates the segments as correction units together with an aerial photo and a Landsat scene used for the correction. This segmentation was exported as a polygon shapefile with each Landsat/photo ratio as a data field in the attribute table.

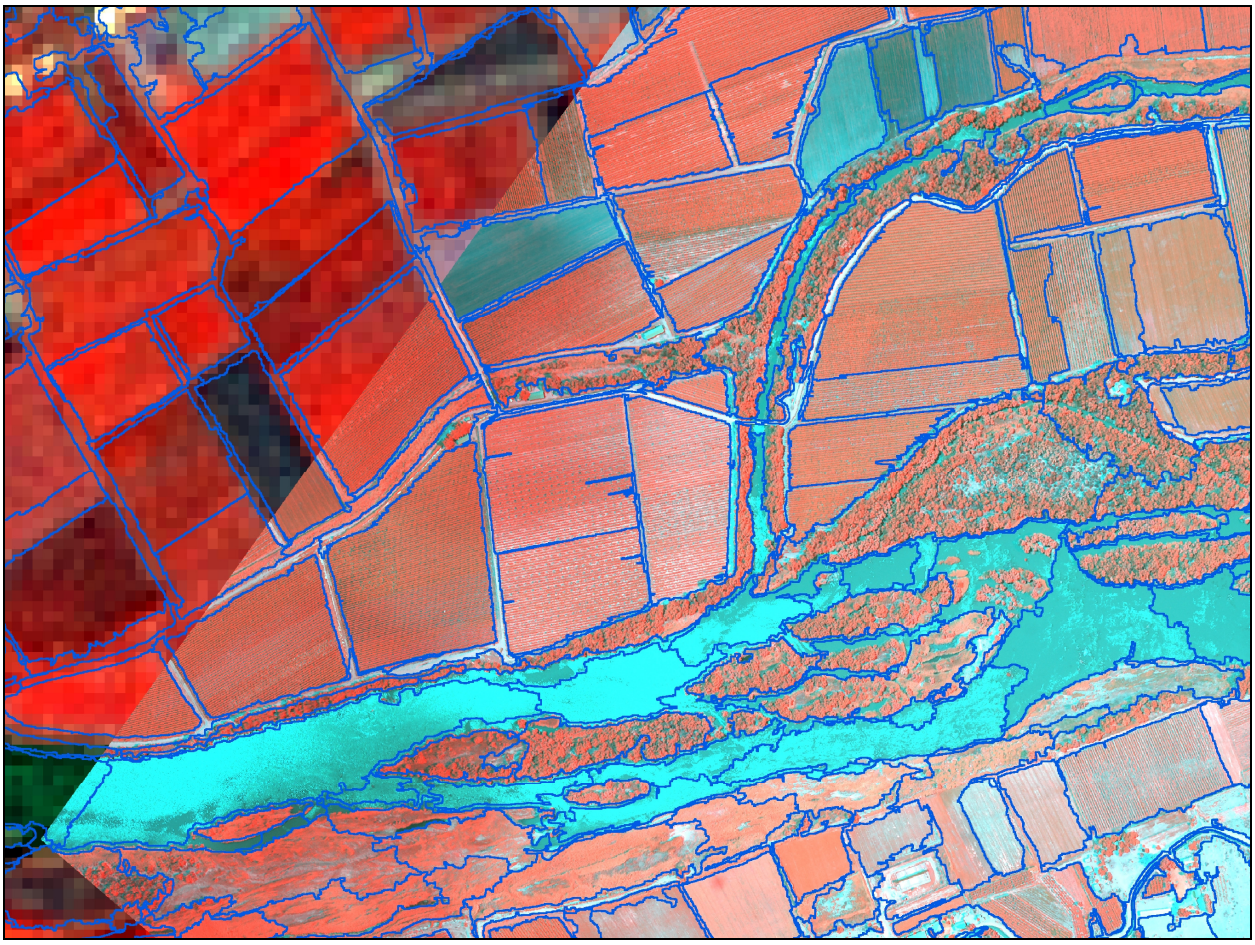

Figure 3.3. An aerial photograph over the Landsat ETM+ image and a segmentation

This shapefile was converted to a 0.75m grid for each data field in the table of band ratios between the satellite mean and aerial photo mean per segment. The grids were imported into Erdas Imagine 8.7 as .img files. These .img files were then input into an Erdas model that multiplied the ratio .img files with the original aerial photos ($E_{chi}(x,y)$ in equation (1)) on a pixel per pixel basis for each band. Then the model stacked these new adjusted RGB and NIR bands together with the original edge detected band (5) into a new radiometrically corrected 5 band photo image. Visual inspection of the corrected photos showed satisfying results. Figure 3.4 illustrates two photos before (a) and after (b) radiometric calibration. Notice the absence of the illumination difference at the border between the two overlapping images in Figure 3.4(b).

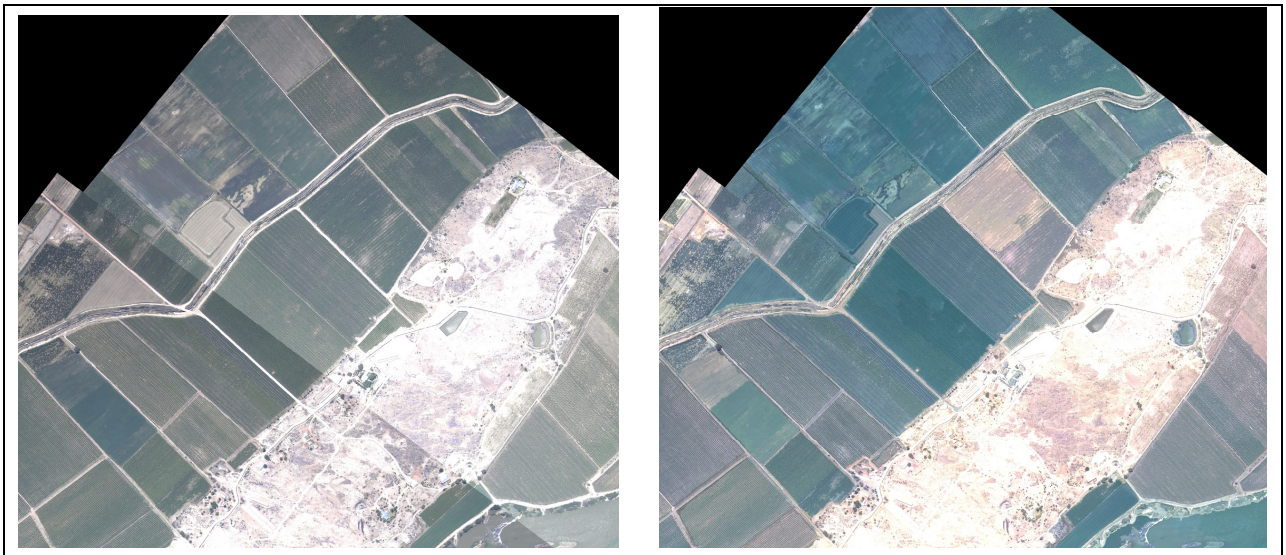

(a) *(b)*

Figure 3.4. A raw (a) and a radiometrically calibrated (b) aerial photograph

3.5 MOSAICKING

The next step was to mosaic the photos for the six different Analysis Blocks into six mosaics. Mosaic testing was conducted in Erdas Imagine 8.7. Visual inspection of the mosaic result was used to assess applicability of a mosaic strategy.

To test the overlap functions in the mosaic process, Analysis Block 2 was selected. It contained some faulty spatial matching between photos from orthorectification in some areas and had many areas where more than two photos overlapped. It was thus deemed a proper block for testing the mosaic results. The "Average" overlap function produced good results but had thin black lines at the regions where the top photo edges in the mosaic were situated. The "Feathering" overlap function produced better visual results in the areas of imprecise spatial overlap in Analysis Block 2 and also fewer black lines at the photo edges. It was decided to mosaic all the Analysis Blocks using "Feathering" as the overlap function. All six Analysis Blocks were mosaicked and is henceforth called Mosaic 1 to 6. Figure 3.5 shows the mosaic result for Analysis Block 2.

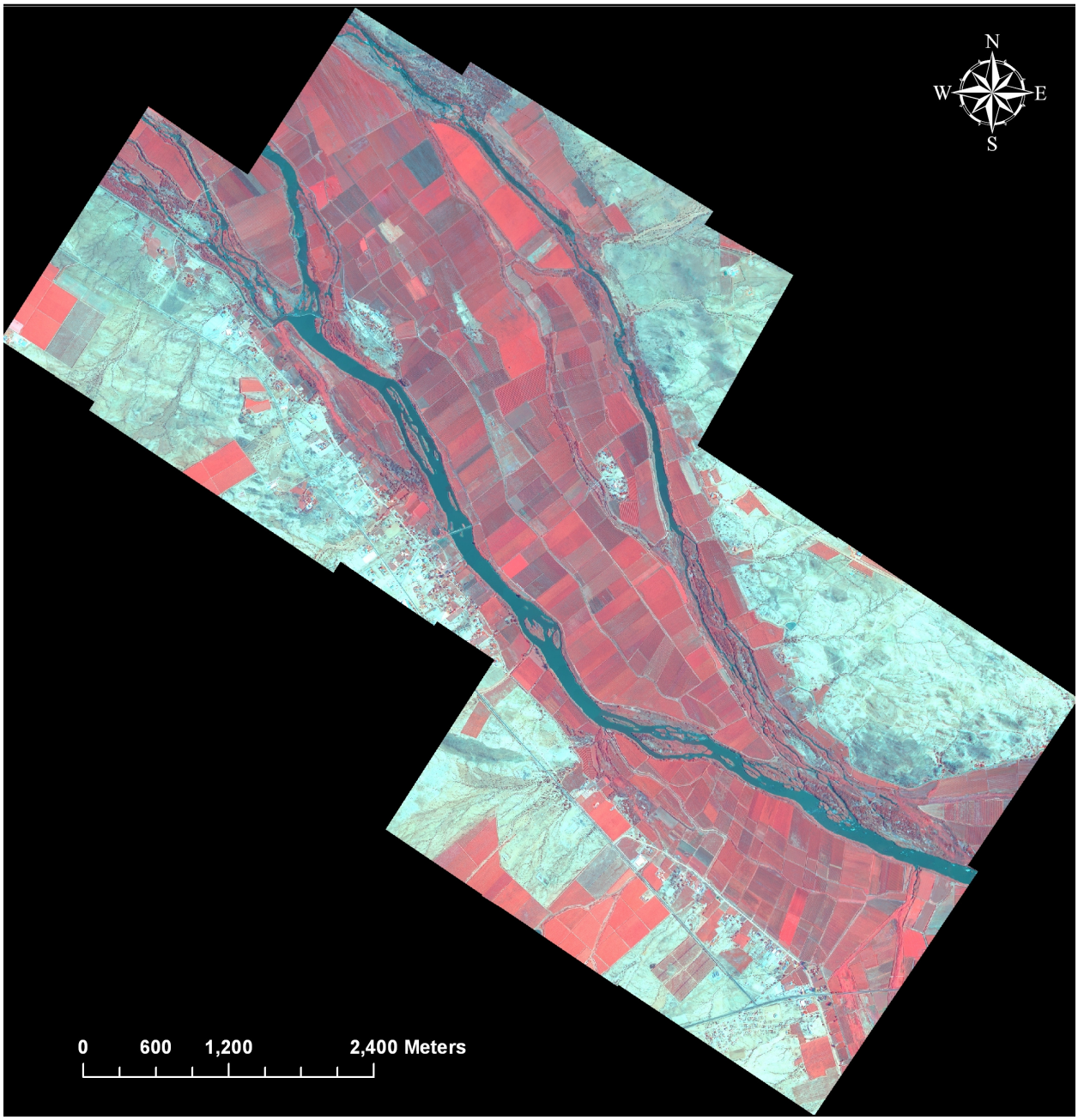

Figure 3.5. The result of the mosaic process for Analysis Block 2 displaying a 4, 2, 3 band combination.

This chapter described the processes conducted on the raw data to prepare it for object-oriented image classification. The following chapter describes how the rule bases for the classification were created and the image classification accuracy assessment conducted.

4: RULE BASE CREATION AND CLASSIFICATION

This chapter reports on the implementation of object-oriented image analysis for detecting soil salinization. The following sections give an explanation of how the segmentation was done and the rule base was created for classifying salinized areas.

4.1 CLASSIFICATION STRATEGY

The strategy used for the research was to create the rule base on one Analysis Block and export and implement it on the other blocks. Thus a transferable rule base was created on a calibration area (Analysis Block 1) and implemented for automated classification on the other Analysis Blocks.

Informational classes are defined as categories of interest to the user of the data. Spectral classes are pixel groups with similar brightness in several spectral channels (Campbell 2002). The informational class required for the research was areas of potential soil salinization. This informational class was determined through two data sets, digital aerial imagery and DEM's. Campbell (2002) states that image classification is the matching of spectral categories to informational categories.

The spectral classes present in the digital aerial photography could be matched to weak vegetation vigour, which is one of the responses of vegetation to highly saline soil as discussed in Chapter 2. The possibility for object-oriented image analysis to detect non-homogenous sites inside a class of classified objects, such as agriculture fields, was explored. This capability was exploited to detect weak growth vigour areas in irrigated farmland. The ability of eCognition to use shape and contextual information in the classification process added another dimension to the image classification. Another phenomenon where salinization is likely to occur is in areas of entrapped drainage as discussed in chapter 2. To detect this indicator the DEM's were used.

Because of the huge differences in spatial resolution between the imagery (0.75m) and the DEM's (25m) problems occurred with segmentation using both datasets together in exploratory classifications with eCognition. It was decided to create different rule bases and separate classifications for the vegetation response to the salinization indicator and the terrain indicator.

The rule base was created on one Analysis Block and applied to the other blocks in order to judge the effectiveness of automated classification using rule bases. Mosaic 1, the aerial image mosaic for Analysis Block 1, was chosen as the Analysis Block to create the rule base for vegetation classification. The extent of Mosaic 1 was small, but contained enough variability of the land cover features found in all of the other mosaics. The terrain rule base was also created on the DEM of Analysis Block 1. The capability for hierarchical object segmentation and classification offered by object-oriented classification was explored in the creation of both rule bases.

4.2 VEGETATION RULE BASE

The following strategy was implemented in each level of segmentation/classification to create a rule base for vegetation stress:

- Define the informational classes first, then create pseudo rules (normal language rules) which may identify each class.
- Segment the image and examine the values of the object features which may define the informational class.
- By using the feature parameters gained from the object feature examination create the classes and the formal rules for the fuzzy sets used for definition of those classes.

Table 4.1 shows the initial informational classes that were defined together with their pseudo rules. These informational classes and their rules were not necessarily implemented in the final classification, but served as a guideline in setting up the rule based classification hierarchy.

Table 4.1. The initial informational classes defined by their pseudo rules.

Informational class	**Pseudo rules**
Water	Low NIR
Roads/Paths	Length/width ratio
Urban/Buildings/Hard Surfaces	High Brightness, square or rectangular shaped
Open Land	Mostly high brightness especially red band (sand), bushes (texture), River rocks - proximity to water
Riverine vegetation	High Vegetation index, proximity to water
Trees/forest/bushland	High Vegetation index, not fields or orchards, not square or rectangular shaped
Vineyards/Orchards	High Vegetation index, often square or rectangular shaped fields, often rows of vegetation and soil (texture)
Other fields	Growing - high Vegetation Index, Urban grass, Fallow fields - low Vegetation Index, high or low brightness, square or rectangular shaped.

The informational class was a class that needed to be identified using image classification and had to serve as rough land cover features, that could be used as contextual information for better class separation and the definition of finer scale classes. The informational classes in Table 4.1 was derived without considering at which segmentation scale they were likely to occur. The pseudo rules that were used to identify the informational classes were derived from remote sensing literature or by visual examination of the photographs. The pseudo rules can be considered as expert knowledge used by the user to train the object-oriented rule base in identifying the class.

4.2.1 Vegetation Segmentation

To determine the best segmentation parameters is often a labour intensive and time consuming process (Zhang & Maxwell 2006). Many segmentation parameters were tested (different scale, shape, spectral weight etc. parameters). The broad strategy which was followed was to extract individual cultivated field blocks as single objects and then segment the fields into smaller segments. These within field segments would serve to highlight patches of weak growth within a field block. This was eventually achieved with four segmentation levels. The levels and parameters follows in Table 4.2.

Table 4.2. The segmentation parameters used in the vegetation rule base classification

Level	Scale	Colour/Shape	Compactness/Smoothness	Bands and Weights				
				B1	B2	B3	B4	B5
4	200	0.9/0.1	0.6/0.4	0.0	0.1	0.1	0.0	2.0
3	150	0.9/0.1	0.6/0.4	0.0	1.0	1.0	1.0	2.0
2	100	0.9/0.1	0.5/0.5	1.0	1.0	1.0	1.0	1.0
1*	10	0.9/0.1	0.5/0.5	1.0	1.0	1.5	1.0	0.0

* Classification based segmentation

The following were the reasons for the segmentation parameters that were used in Table 4.2. The colour parameter was more important than shape as the edge detection band 5 aided the definition of correctly shaped objects.

- **Level 4: reasons for parameters:**
    - Scale: need to classify field blocks, large extent.
    - Compactness: blockier shapes needed for field block objects.
    - Band weights: B5 delineates field block borders; B2,3 indicates areas of vegetation.
- **Level 3: reasons for parameters:**
    - Scale: field blocks and smaller field blocks.
    - Compactness: blockier shapes needed for field blocks and dams.
    - Band weights: B5 for field blocks, B2-4 increased for water and vegetation growth differentiation from soil (NIR, red, green).
- **Level 2: reasons for parameters:**
    - Scale: field blocks kept, other features often included in field block segment at Level 3 were segmented out such as inter block pathways.
    - Band weights: B1-5 equal weights to differentiate spectral differences between field blocks and surrounding features such as pathways.
- **Level 1: reasons for parameters:**
    - Scale: individual rows in vineyards segmented as well as patches in field blocks with total vegetation cover.
    - Band weights: B3 – sand in region has strong red reflection and vegetation absorbs red wavelengths, the NIR is not always well aligned with RGB image in the stack, red is good for differentiating vineyard rows from soil in between rows; B5 - no need for field block edge weight in segmentation as field blocks already determined in object levels 2-4.

Note that the level 1 segmentation was conducted as a classification based segmentation. It means that only the objects classified as a certain class(es) at level 2, with those classes defined in a structure group (in this case objects classified as fields), will be segmented at level 1 (Baatz et al. 2004). The reason for this is that only field blocks will be analyzed for vegetation stress and any subsequent segmentation of other objects would be redundant.

A subset of Analysis Block 1 with the three finer levels of segmentation is illustrated in Figure 4.1.

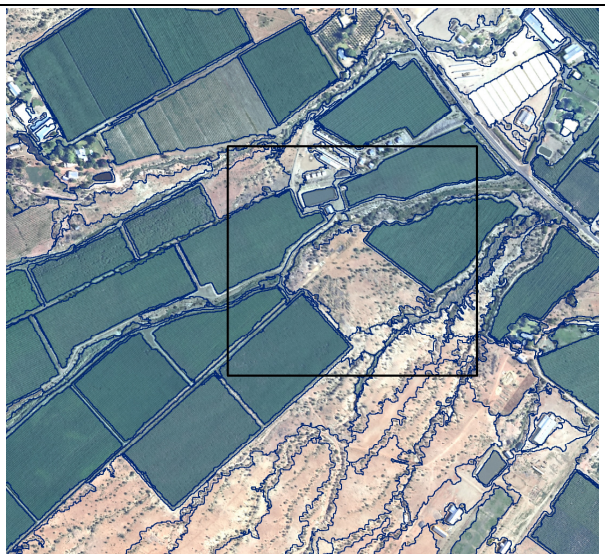

(a) level 3

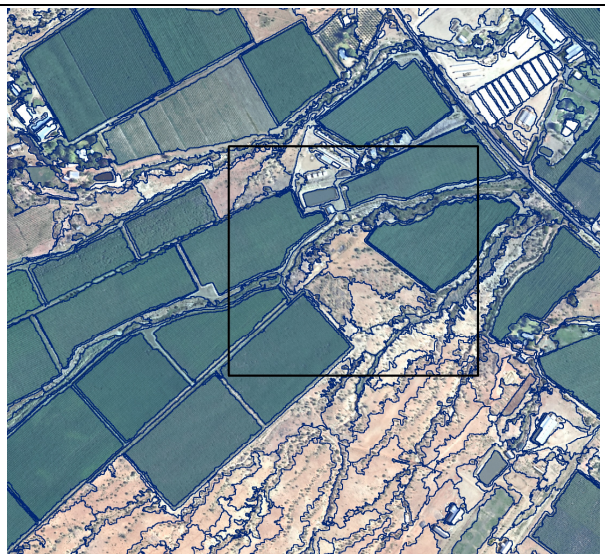

(b) level 2

(c) level 1

The black box in *(a)* and *(b)* is the area zoomed to in *(c)*.

Figure 4.1. Segmentations at 3 different scales

Note that the segmentation was barely different between level 3 (a) and level 2 (b) in the field blocks. The level 1 segmentation divided fields into either rows or smaller within field blocks (c).

4.2.2 Vegetation Class Hierarchy and Classification

4.2.2.1 Level 4 Classification

The objective of the level 4 classification was to separate objects of abundant vegetation cover from objects of little vegetation cover. A lower NDVI threshold for classifying VEGETATED objects was determined by selecting all level 2 objects found to be vegetated field blocks by visual interpretation and inspecting the lowest NDVI values of the selected objects. A membership function with an increasing sinusoidal curve (see Figure 4.2a) for the feature "NDVI" was used to define the class VEGETATED objects.

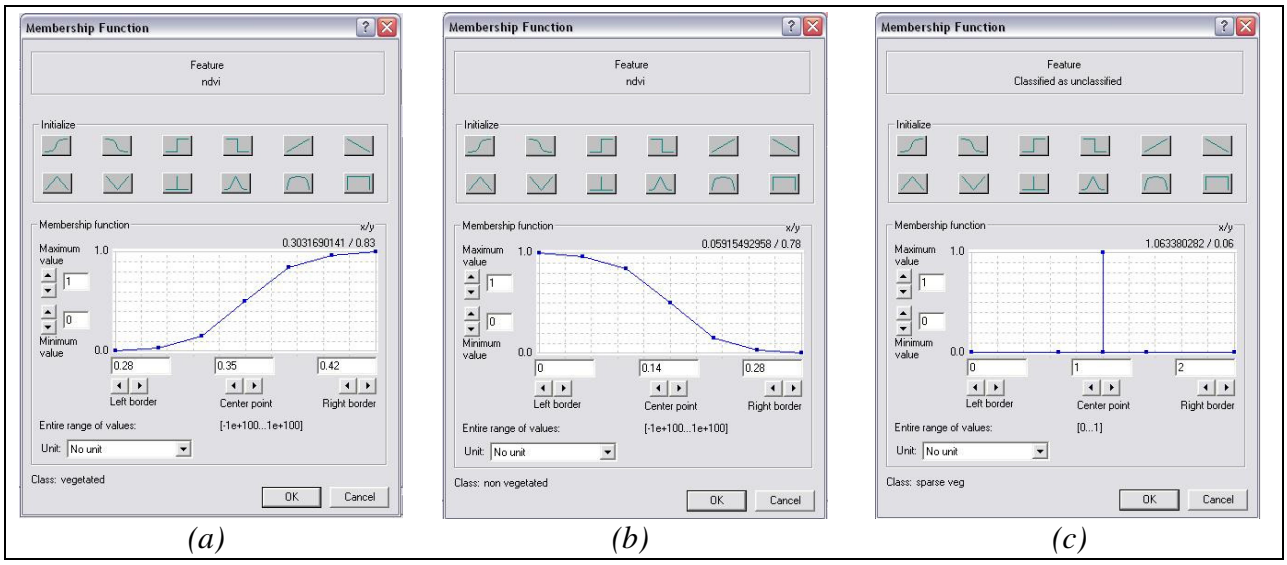

(a) *(b)* *(c)*

Figure 4.2. Membership functions with positive and negative sinusoidal curves and a crisp function

The function had a lower threshold for membership 0 at 0.28 NDVI and upper value where membership equals 1.0 at 0.42 NDVI. The class NON-VEGETATED had a declining sinusoidal

curve function with upper threshold at NDVI 0.28 giving membership 0.0 and an NDVI of 0 giving a membership value of 1.0 (see Figure 4.2b). It was decided to create a class SPARSE VEGETATED which will occupy the fuzzy area of NDVI values along the upper NON-VEGETATED threshold and lower VEGETATED threshold. The contextual rule “classified as unclassified” was used to define this class (see Figure 4.2c).

4.2.2.2 Level 3 Classification

For level 3 a rough land cover classification was created. For determining potential salinization only the agricultural field blocks (class FIELD BLOCKS at level 3) were to be analyzed for vegetation stress, but a rough land cover classification was needed as well. The reason for this was to create more classes to serve as contextual information for more accurate classification of the desired features (fields). It also helped to separate objects with similar feature values from incorrect assignment to FIELD BLOCKS. For example forested areas and riparian vegetation could be excluded a posteriori. As another example, for the definition of RIVERINE VEG the class WATER was needed. The WATER class could be extracted from the generalized land cover segmentation at level 3. Figure 4.3 shows the level 3 rough land cover classification for Analysis Block 3.

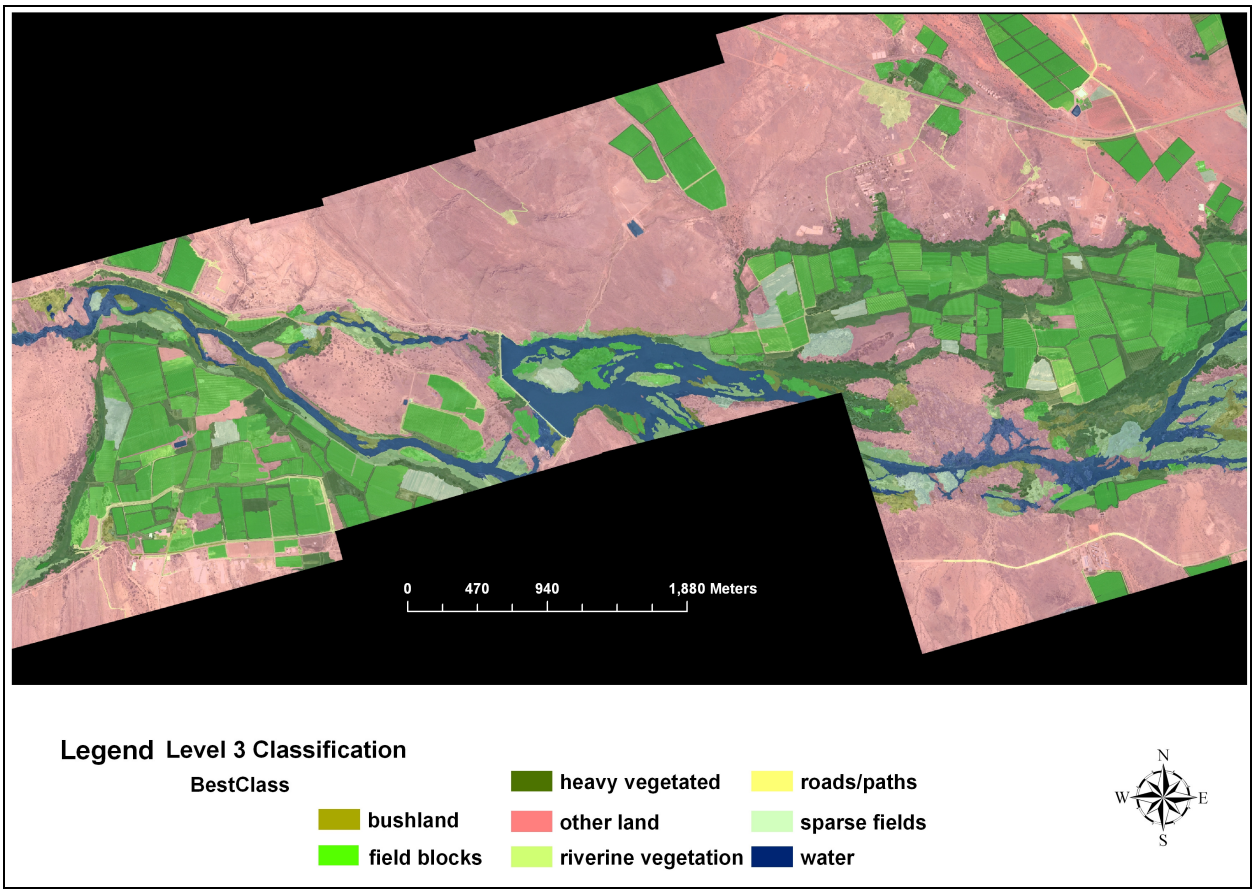

Figure 4.3. The rough land cover classification at segmentation level 3

The feature view, which displays the objects of the feature value under investigation in greyscale (see Figure 4.4), was used for the definition of many membership functions for class rules at this level. In Figure 4.4 the band 4 (NIR) value was investigated for defining the class WATER. Higher feature values (NIR) for objects are white while lower values appears darker or black. This method was used to determine the upper threshold in NIR for water bodies to create the WATER class.

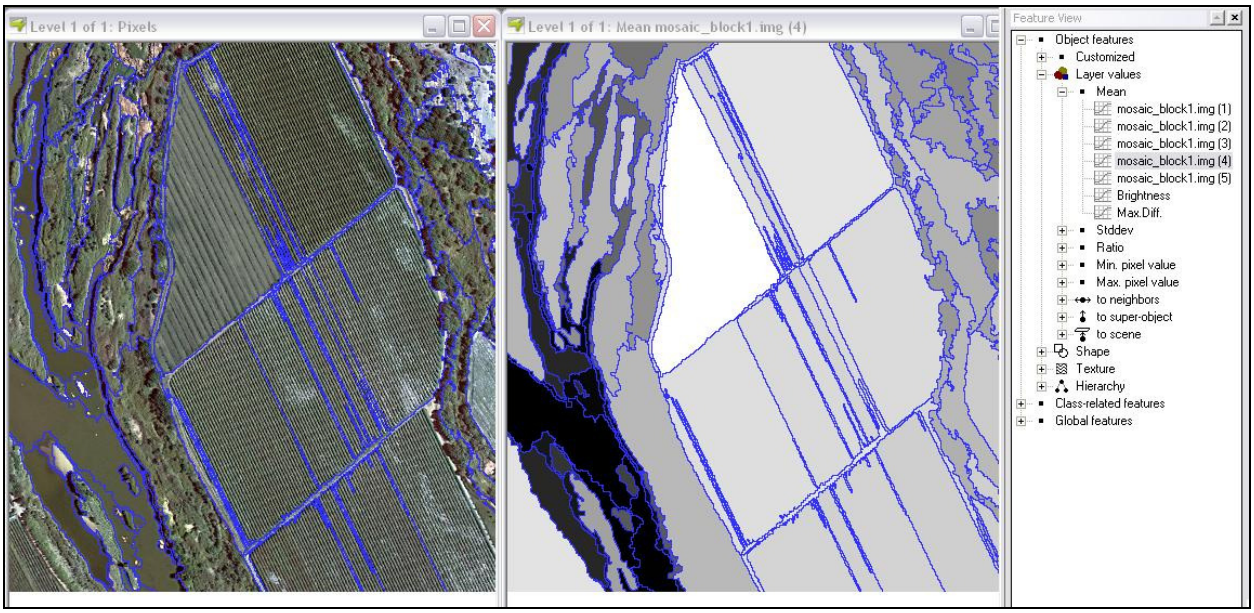

Figure 4.4. The feature view was used to find the values of objects in order to define the membership functions of classes

The feature view was also used to determine the feature values for "compactness" and the "shape" indicator, that would determine the membership function for these expressions defining the class FIELD BLOCKS. The contextual rule "existence of VEGETATED super object" was also used to keep FIELD BLOCKS within objects of sufficient vegetation (class VEGETATED at level 4). It was defined by the classification of the larger object level above. The class SPARSE FIELDS was defined the same way as FIELD BLOCKS but had SPARSE VEGETATION super objects and lower NDVI values. The purpose of this class was to identify agricultural fields of very low vegetative cover.

With the important class defined for level 3 (FIELD BLOCKS) the next classes could be defined to differentiate incorrect objects from this class. The class HEAVY VEGETATED consisting mostly of forested areas were defined again using the feature view. The feature rules for this class were "existence of VEGETATED super objects", "not classified as FIELD BLOCKS" and an NDVI value with the same membership function as was found for the class VEGETATED in level 4 above. The class BUSHLAND was defined using the standard deviation of the super object for the NIR band and also limiting the class to super objects classified as SPARSE VEG. RIVERINE VEG was created by limiting the class to objects classified as VEGETATED in the super objects in level 3 above and by giving a minimum distance of 5m to neighbour objects

classified as WATER. RIVERINE VEG super objects had to be classified as VEGETATED at level 4 and with an increasing sinusoidal curve membership function from 0 to 1.0. The objects must be “not classified as FIELD BLOCKS” and “not classified as WATER”. These classes were often mistakenly assigned to objects which should be RIVERINE VEG.

An attempt was made to classify fallow fields (non-vegetated field blocks) by selecting samples of objects of this class. The sample objects used in the subsequent classification of fallow fields could not be differentiated from other land cover types (such as open natural areas) and the class was dropped. The class OTHER LAND was defined by positive sinusoidal curve membership functions from 0 to 1.0 as being “not classified as…” FIELD BLOCKS, WATER, HEAVY VEG, BUSHLAND, RIVERINE VEG, etc.

4.2.2.3 Level 2 Classification

The segmentation at level 2 had the purpose to better delineate field blocks, therefore higher band weights were assigned to all the spectral bands and a lower weight to the edge detected band. The reason was to exclude non-field block type objects, such as paths between blocks which were included at level 3. Another reason was to reclassify incorrectly classified HEAVY VEGETATION in level 3 from the BLOCKS class - the class defining the agricultural fields under investigation at level 2. To achieve this, the BLOCKS class rules contained the OR operator which divided the rules to the class into two sets of rules. The first set was designed to reclassify incorrect HEAVY VEG objects at level 3 by determining that its super object should be classified as HEAVY VEG. It had the same “shape” and “compactness” feature values as those found defining field blocks in level 3. The other rule set on the other side of the OR operator determined that the super object should be classified as FIELD BLOCKS (the correct classification at level 3).

Another class, BLOCK PATHS, was created to exclude segments which were part of FIELD BLOCKS in the super object and in reality were the thin paths or spaces between agricultural field blocks. Some of these paths between blocks were also classified wrongly as HEAVY VEG in level 3 (see Figure 4.3). The rules “existence of HEAVY VEG super objects” and “relative

area of BLOCKS neighbour objects" were used to define this class. SPARSE BLOCKS was, as in Level 3, the same as BLOCKS but with SPARSE FIELDS super objects and lower vegetation cover.

4.2.2.4 Level 1 Classification

The objective for classification at the finest segmentation scale is to separate vegetation cover within a BLOCKS super object from visible soil between the vegetated rows or to divide a fully vegetated BLOCKS object into patches of vegetation that might produce high within field NDVI variability. The vegetation objects per block can then be analyzed to determine areas of weaker growth within the block by analyzing average NDVI values for the blocks. The vegetated objects that deviate from the average NDVI for vegetation in the field block can then be determined. The weaker NDVI vegetated objects could then serve as definition of weak growth patches and as indicators of possible salinization.

Many different classification strategies were explored to classify objects at this level. Field block vegetation had to be separated from bare soil within a block. The problem with these objects at this pixel resolution was that the vegetation within a field block appears in many forms. Johnson et al (2003) notes the challenges in remote sensing of vineyards. Highly discontinuous canopies, clumped foliage along individual vines or rows, low overall ground cover fraction, understory foliage as cover crop or weeds, and different canopy architecture among fields because of different trellis systems are some of the problems encountered in remote sensing of vineyards. Some field blocks have vegetation rows, mostly vineyard fields, while other fields also have vineyard rows, but with closed canopies making no soil visible from above. In Figure 4.5a the central field shows a closed canopy on the left and open rows on the right. Other fields had non-vine vegetation cover which contained other variability in the appearance of the vegetation cover. These problems resulted in a detailed rule base of rule sets where the true potential of object oriented analysis for high resolution precision classification was exploited. An explanation of the classes and rule sets follows.

(a) *(b)*

Figure 4.5. The problems of varied vineyard appearance

Sample objects of BLOCK VEGETATION and BLOCK SOIL were chosen using eCognition's sample editor. From the sample editor membership functions for the 4 spectral bands were automatically created and inserted into these classes (see Figure 4.6). In the figure the white samples are rows of BLOCK SOIL and the green BLOCK VEGETATION. The histograms on the right are the values for the different bands as well as vegetation indices for the sample objects. Membership functions were generated from this sample editor and inserted into the class definitions as rule sets.

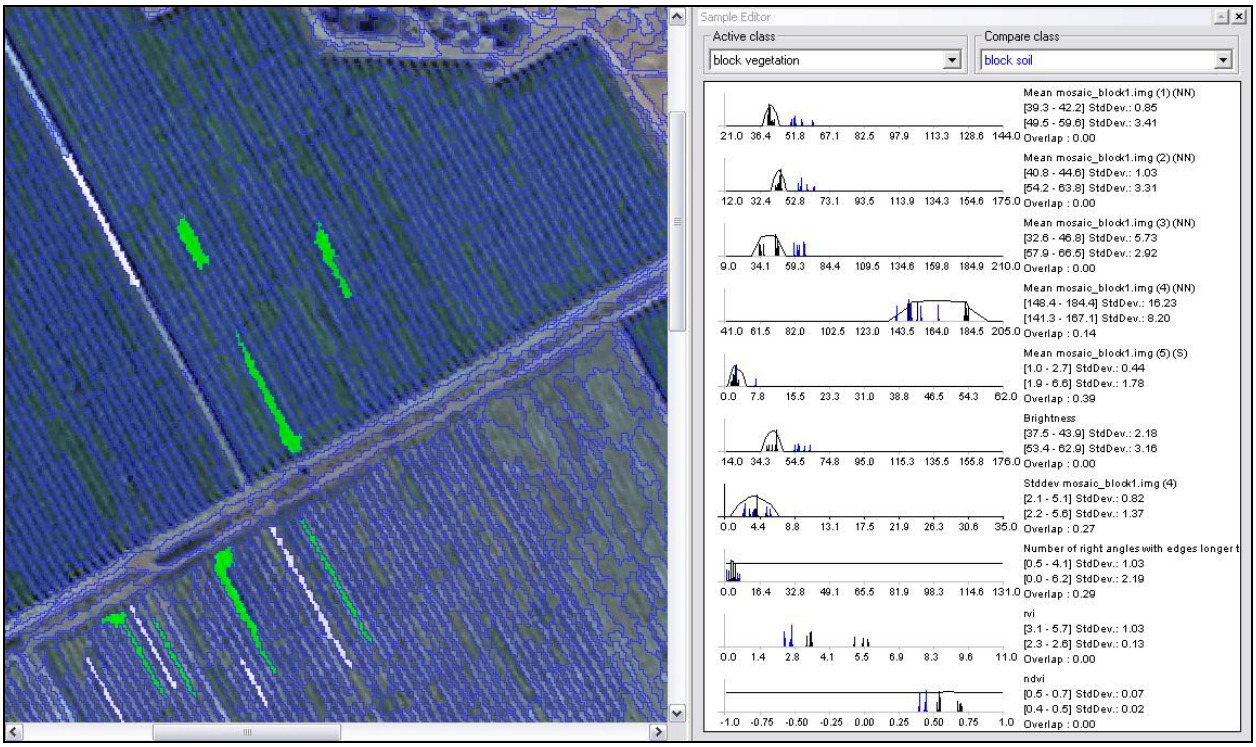

Figure 4.6. An example of how samples are chosen for the class BLOCK VEGTATION (green) and BLOCK SOIL (white)

One problem arising with objects at this fine resolution scale was that some sample objects which were identified by the user as very sparse vegetation rows are often confused with soil objects. The need to include these sparse rows is clear because of the considerable variability of vegetation growth stages and cultivation practice within field blocks. The confusion of sparse vegetation row sample objects with soil objects could be ascribed to the mixed pixel problem (Campbell 2002). See Figure 4.5b for an example of very sparse rows. At a spatial resolution of 0.75m the digital aerial photography pixels for sparse vegetation rows also picks up spectral response from the soil within the field block.

The initial classification of BLOCK VEGETATION and BLOCK SOIL used a nearest neighbour classifier for the sample object derived membership functions and the membership rule that determined the existence of a BLOCKS super object, thus keeping the objects within agricultural field blocks classified at level 2. The Feature Space Optimization tool was used on the samples to determine which features best separated the class BLOCK SOIL from BLOCK VEGETATION (example in Figure 4.7). The Blue and Green bands as well as total Brightness

(defined as Red, Green and Blue bands combined) as well as the Ratio Vegetation Index (RVI = NIR/Red) gave good separation of the classes from the sample objects. An increasing sinusoidal curve membership function for the possible NDVI for BLOCK VEGETATION and a declining sinusoidal curve membership function for BLOCK SOIL NDVI values were defined as rules for these two classes.

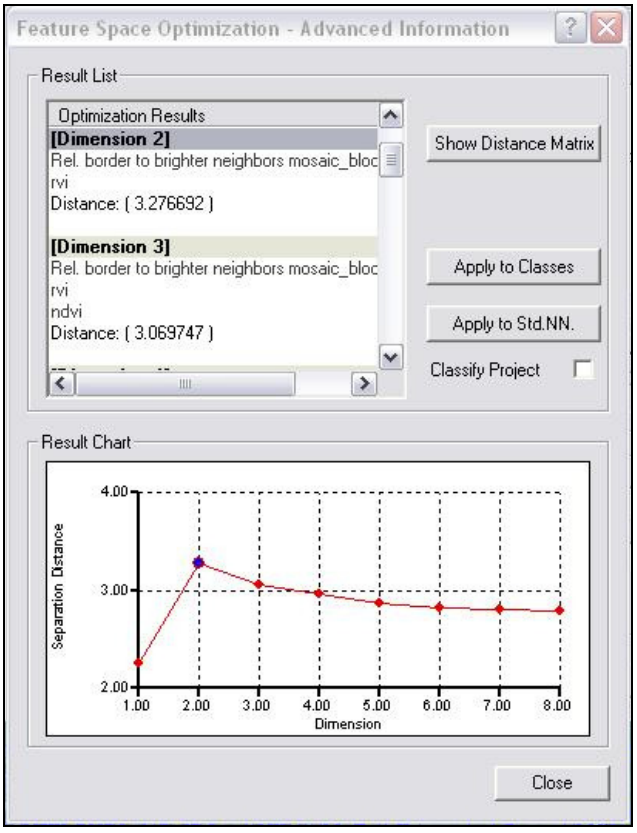

Figure 4.7. The Feature Space optimization tool

The Feature Space optimization tool is used in this instance to calculate the maximum separation possible between BLOCK SOIL and BLOCK VEGETATION by using a certain number of selected features. In this case the two features "Relative border to brighter neighbors (band 3)" and "RVI" were the two features which could be used for best separation of the samples. Note that more than 2 features would have reduced the seperability of the two classes as is visible from the graph.

The classes SPARSE BLOCK VEGETATION and SPARSE BLOCK SOIL was based on SPARSE super objects. The amount of SPARSE objects classified was insignificant to warrant further analysis of the SPARSE classes at its different levels in the hierarchy.

The initial classification produced erroneous BLOCK VEGETATION objects which should have been classed as BLOCK SOIL, largely because of the mixed pixel problem mentioned earlier. This problem mostly occurred between vineyard rows. Extra rule sets were added to differentiate BLOCK SOIL from BLOCK VEGETATION. The feature "relative border to brighter neighbours" held promise if inverted ("NOT" was added in front of the expression to the feature,

giving the inversion of the expression result) and applied to BLOCK VEGETATION in the NIR band. Figure 4.8 shows how this feature appeared in the feature view. The reasoning behind this is that vegetation has stronger reflectance in NIR than soil. The rectification and stacking of the NIR photographs on the RGB photographs were not always exact and meant that strong NIR rows did not always fall correctly on the RGB vineyard rows. The Red band (3) was then applied for this purpose as vegetation absorbs red wavelength energy whereas the red sand and soil should reflect a large proportion (Campbell 2002).

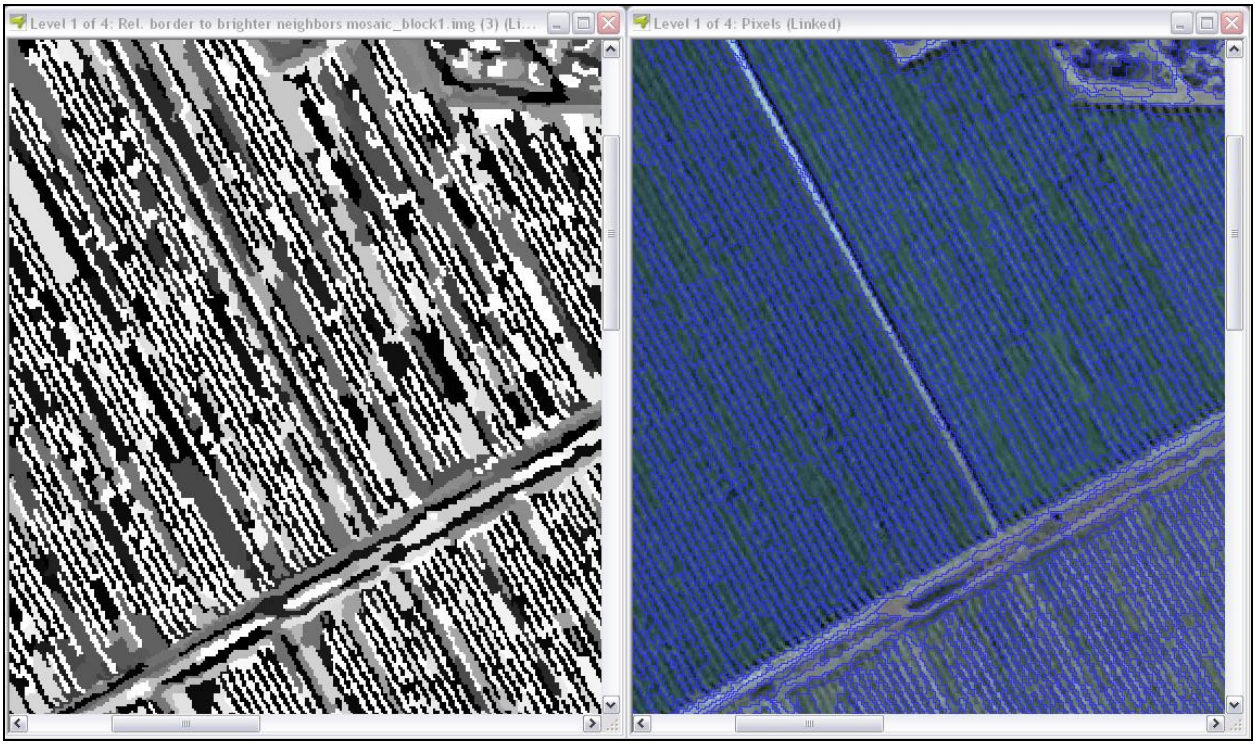

Figure 4.8. The feature view for "relative border to brighter neighbours band (3)"

An inverted rule set producing the minimum of the asymmetry of the object (which defines a long shape, such as a vineyard row) and the relative border to brighter neighbours for band 3 was added to the BLOCK VEGETATION class. This rule set managed to successfully keep soil objects between vegetated rows from being classified as BLOCK VEGETATION.

Initially an attempt was made to create a subclass within BLOCK VEGETATION that would indicate areas of weaker NDVI values for vegetated objects within a field block. It was decided to analyze the vegetation within a field for vegetation stress whilst leaving out the soil within the field from the stress analysis. See Figure 4.9 for an illustration of the BLOCKS and BLOCK

VEGETATION and BLOCK SOIL objects. The eCognition program has the capability for the user to create customised features. By creating customised features it was possible to calculate the average NDVI for the objects of vegetation (BLOCK VEGETATION, See the green objects in Figure 4.9a) within individual BLOCKS super object (see the green objects in Figure 4.9b with the red indicating the border of an individual BLOCKS object). Thus any exposed soil such as visible rows of soil objects in between vineyard rows (see the grey objects in Figure 4.9a) were excluded from vegetation NDVI analysis within a BLOCKS object. The standard deviation for the BLOCK VEGETATION objects per BLOCKS super object was also calculated.

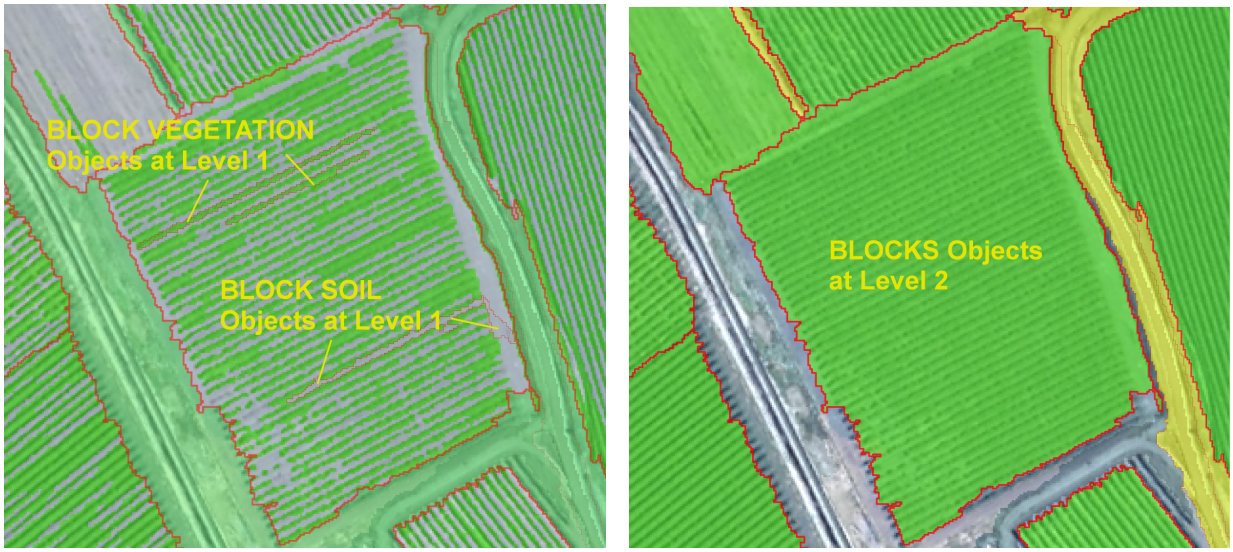

Figure 4.9. The classified field level objects at different segmentation levels

The final feature, the Z value of each individual BLOCK VEGETATION object within a BLOCKS super object was also calculated. The Z value served as an indication of the deviation of the vegetated sub objects from the average NDVI of all the vegetated sub objects located within each BLOCKS object. The Z value is defined in equation 2 as follows:

$$Z = (ndvi_{vegobj} - avg.ndvi_{blockveg}) / stdv.ndvi_{blockveg} \qquad (2)$$

The $ndvi_{vegobj}$ is the NDVI value of a single object of class BLOCK VEGETATION. The average NDVI for all level 1 objects classified as BLOCK VEGETATION contained in a BLOCKS super object (thus all vegetation in the field) is indicated by $avg.ndvi_{blockveg}$. The standard

deviation of these BLOCK VEGETATION objects in the field is indicated by $stdv.ndvi_{blockveg}$. Thus the Z value gives an indication of NDVI variability from the average of the field.

Lower Z values indicated areas of vegetation stress within a field block as defined by a BLOCKS classified super object. It was found that to calculate Z value thresholds to define a new class for stressed vegetation that was applicable over all the Analysis Blocks was not feasible. This was due to many micro sized objects present that had especially low Z values. These objects were often located at the edges of agricultural fields where small objects were segmented and classed. The objects at the field edges often contained mixed pixels or in some cases had inaccurate spatial overlap between the RGB and NIR photos during the stacking and mosaicking phases. This caused low NDVI values and these small edge objects to be outliers in the histogram of Z values. To determine Z value thresholds these edge object outliers had to be left out of Z value threshold calculations (their small size made their removal insignificant to the calculation) and could be conducted in GIS. The Z value was thus exported with the level 1 classification as a field in the shapefile table to be used in defining vegetation stress by GIS. It was then decided to follow the same procedure for all Analysis Blocks.

4.3 TERRAIN RULE BASE

The terrain rule base was applied to the DEM of the area and contained much less complexity than the rule base for vegetation. According to the literature the topographical features that needed to be classified using the height data were areas of entrapped drainage. These areas hold potential for possible soil salinization. Utset & Borroto (2001) found in their study that areas of higher salinity in irrigated lands are those of lower elevation. These lower areas in the terrain caused a rise in saline groundwater in the water table as the downward lateral flows from irrigated lands accumulated there. Rezaei & Gilkes (2005) also reported that leached salts collect in lower terrain areas.

4.3.1 Terrain Segmentation

Several exploratory segmentations were conducted to derive good segmentation parameters. Because of the coarse resolution of the DEM (25m) it was decided to start segmentations at the finest scale (scale parameter 1). Attempts to find entrapped drainage at this smallest scale parameter was then followed by subsequent segmentations and classifications and increasing the scale parameter in the object hierarchy. Finally six segmentation levels at scale parameters 1, 2, 5, 10, 20 and 40 were created. The shape parameter for all segmentations was 0.1 and smoothness and compactness were 0.5. Only one class that defined areas of possible salinization was created for each object segmentation level in the hierarchy.

4.3.2 Terrain Classification

The classes created for identifying terrain features were MICRO DEPRESSIONS at level 1 (scale 1 – the finest segmentation), MINI DEPRESSIONS at level 2, SMALL DEPRESSIONS at level 3, SMALL BASINS at level 4, MEDIUM BASINS at level 5 and LARGE BASINS at level 6. All the DEPRESSIONS classes and all the BASINS classes had exactly the same rules applied to their features, only the scale of the objects being classified was different. Argialas and Tzotsos (2006) used DEM Slope as another layer in a knowledge based classification of landforms. Because most of the area in which salinization was searched for in this study was a relatively flat river floodplain, it was not deemed necessary to use a Slope image in classification. .

Only one feature was used to define each of the classes: “relative border to brighter neighbours”. As the DEM which was segmented corresponds to height, with higher elevation values showing increasing brightness, this rule was sufficient. Thus objects which were bordered by brighter (higher) neighbour objects would indicate areas of lower elevation. BASINS and DEPRESSIONS are illustrated in Figure 4.10 over a DEM.

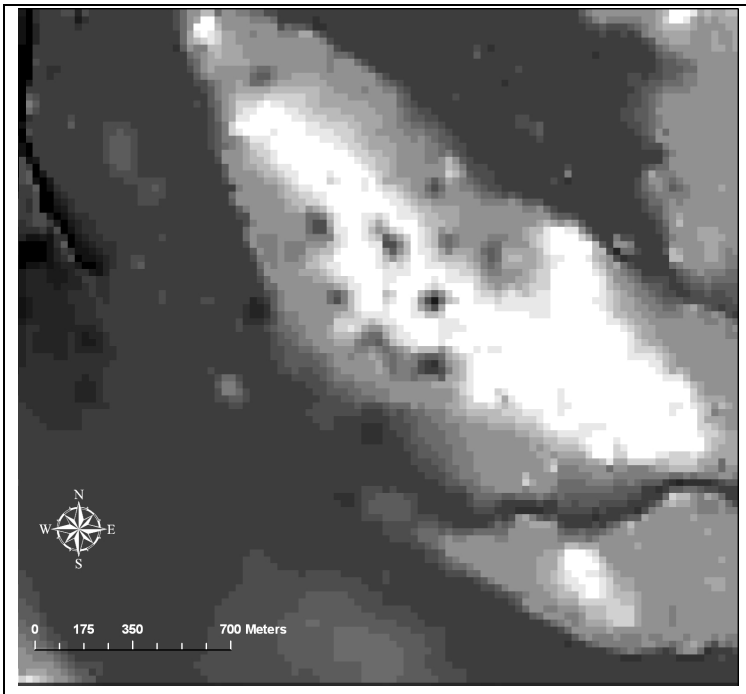

a) A DEM used for the classification of BASINS and DEPRESSIONS. Note the dark spots indicating areas of lower elevation than its surroundings.

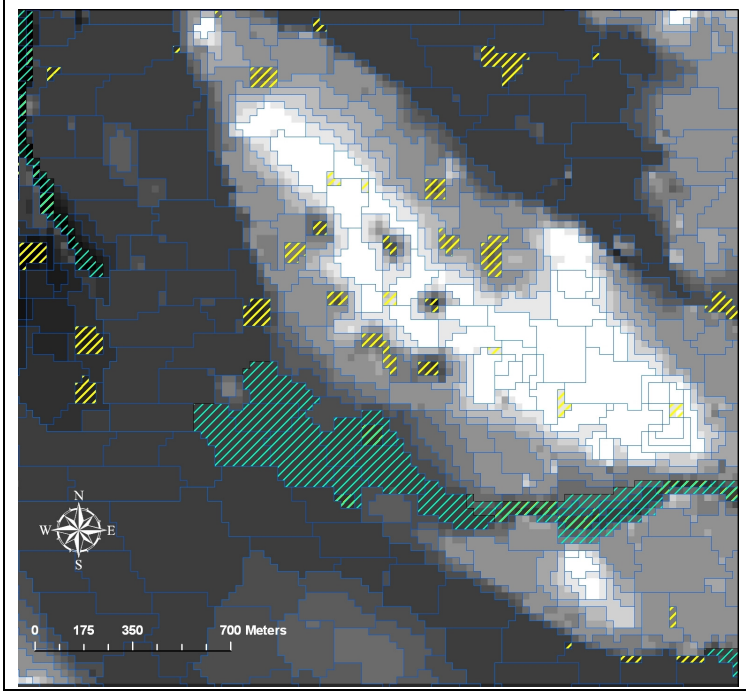

b) The same DEM as in *(a)* but with the classifications of a BASINS class (green) and DEPRESSIONS class (yellow) as diagonal stripes overlaid. The segmentation borders are shown in blue. Non-striped segments were not classified as either BASINS or DEPRESSIONS.

Figure 4.10. The DEM, segmentation and classification of the terrain salinity indicators

The membership function for the DEPRESSIONS class determined that the relative border to brighter neighbours was a crisp (not fuzzy) classification and should be 1.0 giving a membership value of 1.0. Thus it defines an object that had brighter (higher) neighbouring objects along its

whole border length. It is therefore a depression in the landscape. The BASINS class had an increasing sinusoidal curve membership function for the "relative border to brighter neighbours" rule. The lower (lesser membership) X value of the function was at a 0.9 relative border value and the upper (full 1.0 membership) value was 1.0 relative border. Thus BASINS were for the most part lower than its neighbours but did allow a very small outlet for flow in the landscape.

4.4 AUTOMATION BY PROTOCOLS

The whole segmentation and classification process for the vegetation and terrain aspects were recorded in a protocol. The protocol editor in eCognition provides the capability to save and execute image processing steps automatically (Baatz et al. 2004). Once all the segmentation and classification procedures were defined and found to be correct, the class hierarchies and customised features were saved. A new project was started loading in the same data for Analysis Block 1 and the protocol editor was set to record image processing steps followed for an image classification. These steps comprised loading the customised features, the necessary class hierarchies, setting of segmentation parameters and subsequent segmentation and classification at the appropriate levels.

After the automatic classification of all the levels, the classifications were exported as ESRI shapefiles (GIS ready information) for the creation of salinity potential spatial data. The protocol created from the determination of segmentation and classes for Analysis Block 1 was then applied to the remaining 5 Analysis Blocks and the classification results exported.

4.5 IMAGE CLASSIFICATION ACCURACY ASSESSMENT

Accuracy is defined by Campbell (2002) as "…the agreement between a standard assumed to be correct and a classified image of unknown quality." To test the accuracy of the object-oriented image classification a number of methods were followed. Accuracy assessment tools offered by eCognition are: the Classification Stability, Best Classification Result and Error Matrices by either Training or Test Areas (TTA) Mask or Samples. The methods of accuracy assessment

used for the project were Classification Stability, Best Classification Result and an Confusion Matrix based on a TTA Mask.

4.5.1 Classification Stability

The classification stability test is a measure of the ambiguity of an object's classification (Baatz et al 2004). The fuzzy classification offered by eCognition means that an object can be a member of more than one class, but in this project only the class with the highest degree of membership was assigned to an object. To test the degree of membership difference between the best and second best class assignment to objects, the classification stability functionality in eCognition is used. A value for classification stability (1.0 for non ambiguous to 0.0 for totally ambiguous) is calculated. This value is an indication of how much higher the membership value of the best classification for an object is than the membership of the next best classification. The classification stability for all Analysis Blocks with the average of all the regions is displayed in Table 4.2.

Table 4.2. Classification accuracy for the fuzzy classification of agricultural field and vegetation types.

	Best Classification Result		Classification Stability	
Class	**Average**	**Std Dev**	**Average**	**Std Dev**
Level 1				
block soil	0.79	0.21	0.54	0.29
block vegetation	0.97	0.1	0.71	0.31
sparse block soil	0.87	0.16	0.84	0.21
sparse block vegetation	0.76	0.18	0.58	0.28
Level 2				
blocks	0.88	0.28	0.87	0.28
Level 3				
field blocks	0.38	0.16	0.38	0.16
sparse fields	0.57	0.15	0.14	0.12

The table shows weak stability at level 3 but improvement as the resolution of the segmentation becomes finer. A confusion matrix was used to test the actual classification accuracy.

4.5.2 Best Classification Result

The Best Classification Result serves as an indication of how well the objects of a class fulfil the class description (Baatz et al 2004). Objects are assigned a highest membership to a certain class. The average membership value of all the objects with the highest membership to a particular class is displayed by this eCognition accuracy assessment tool. The value is between 0 and 1.0. Table 4.2 displays the statistics for the best classification result for some of the project classes. The table indicates that class definition was not good at level 3, but improved as the resolution of the segmentation improved.

4.5.3 Accuracy Assessment by Confusion Matrix

No ground truth data was available to evaluate the accuracy of the terrain classification of BASINS and DEPRESSIONS. The vegetation classification however could be tested for accuracy. Because of the large amount of data contained in all six Analysis Blocks, the number of classes contained in all four hierarchical levels and the time required to run these tests, it was decided to assess only one level for one Analysis Block.

Analysis Block 4 was randomly selected for accuracy assessment. The most important informational class which was needed in classifying vegetation stress was agricultural field blocks. To test the accuracy of individual field rows at level 1 of the object hierarchy was not feasible, so the accuracy assessment by confusion matrix was conducted at level 2, the level with the best defined agricultural fields as units of classification contained in class BLOCKS.

In order to create the reference data (TTA mask) against which the classification was tested, the level 2 objects were exported as a polygon shapefile. In ArcGis 9.1 this shapefile was overlaid over the digital aerial photograph mosaic of block 4. The high resolution of the mosaic made it possible to identify the landcover in the polygons visually. All the polygons that overlaid agricultural fields were selected and converted to a new shapefile. The borders of these polygons were then manually edited where they deviated from the fields in the photo. This shapefile of

edited field polygons was converted to GRID and imported into the eCognition accuracy assessment by TTA mask for the creation of an confusion matrix. The confusion matrix is found in Table 4.3.

Table 4.3. The confusion matrix based on the TTA mask

User/Reference Class **Confusion Matrix**	**blocks**	**sparse blocks**	**total number of pixels**
blocks	15400169	789689	16189858
sparse blocks	20790	184498	205288
unclassified	1152434	167951	1320385
Total number of pixels	16573393	1142138	17715531
Accuracy			
Producer	0.9292	0.1615	
User	0.9512	0.8987	
Totals			
Overall Accuracy	**0.8797**		

According to the confusion matrix, the class BLOCKS classification was very accurate with a 0.93 Producer and 0.95 User accuracy. According to Campbell (2002) the Producer's accuracy tells the map producer the amount of the feature on the ground (in this case field blocks) that was correctly classified (93%). The User's accuracy tells the user of the map how much of the feature on the map corresponds to the class on the ground (95% of the BLOCKS class is blocks in reality). This means that although the informational class for field blocks was not well defined at level 3 and potentially ambiguous (Table 4.2 at level 2) the classification was still good when tested at level 2, which was the more important level. For sparse growing field blocks the class did correspond to sparse fields in reality (according to the User's accuracy), but very little of the spare fields in reality was classified as SPARSE BLOCKS (Producer's accuracy). The class SPARSE BLOCKS was not considered as an important class in further analysis.

This chapter described the process of building the rule base for object-oriented classification of potentially salinized areas as well as the accuracy assessments conducted on the vegetation and land cover classifications. The next chapter explains how the classification results were tested against ground truth soil samples to test the accuracy in detecting actual salinization. The classified features were also analyzed against the ground truth data to determine which features

carried the lowest to highest salinity potential. These potentials were used to create salinity potential maps.

5: DETERMINATION AND MAPPING OF SALINITY POTENTIAL

In this chapter the accuracy of the data exported from classification in identifying potentially salinized soil was determined. A salinity potential weight based on the ability of each feature to detect true salinity was calculated for each feature. These weights were used to create salinity potential maps.

5.1 ACCURACY ASSESSMENT OF CLASSIFICATIONS USING GROUND TRUTH SOIL SAMPLES

In this phase of the research, the classifications of potentially salinized areas in the form of shapefiles exported from eCognition were analyzed using a GIS. The data derived was compared to point samples of actual salinization. The locations of actual salinization were in the form of a point shapefile of soil samples taken in the area and analyzed for salinity in a laboratory (Volschenk et al. 2005). The areas of potential salinization on the other hand were derived from the object-oriented classifications of the imagery and reworked into salinity potential maps.

5.1.1 Soil Samples

Soil samples were taken in the study area as part of a WRC funded project to map potentially salinized areas. Half of the samples were taken in areas previously classified with remote sensing as potentially saline and the other half in non-saline areas. The soil sample analysis was conducted to determine the total salt concentration by measurement of the electrical conductivity of the saturated soil water extract (EC_e) and the soluble cations and anions (Volschenk et al. 2005).

The soil sampling in the WRC project took place at 0 – 300 mm, 300 – 600 mm and 600 – 900 mm depths. After drying, sieving and creation of saturated paste extracts, the saturation percentage, pH and EC of the saturated extract (EC_e, dS m^{-1}) were determined. Salinity status

was classified according to the mean EC_e over the whole profile. The salinity threshold value was based on the value determined by Moolman et al. (1999) at 0.75 dS m^{-1} beyond which a yield decrease for grapevine is expected (Volschenk et al. 2005). The result was that out of the 96 soil samples taken in this study area, with the assumption from remote sensing classification that half were saline and the other half non-saline, only 16 samples were found by laboratory analysis to be saline.

5.1.2 Determination of salinity potential

5.1.2.1 Strategy

The different indicators that were classified by the object-oriented rule based method had to be assigned a weight for their potential to indicate soil salinization in the study area. The indicators were the various levels of terrain features (basins and depressions) and two levels of vegetation stress (light and heavy). In order to assign a weight to each indicator, the soil samples were used. Due to the complexity in spatial and temporal distribution of salts and the difference in spatial resolution between the vegetation and terrain indicators it was decided to create four buffer radii around each soil sample (5m, 10m, 20m, 50m). The determination of the salinity potential weights was conducted by examining the frequency of occurrence of various classes within these buffered zones around the soil samples. The small number of saline soil samples meant that all saline soil samples had to be used in order to calculate weights for the classifications.

The Z values in the table fields of the exported shapefiles were used to determine which classified vegetated objects displayed growth stress. The multiple classes of BASINS and DEPRESSIONS classified at different levels of the object hierarchy were analyzed for their contributing potential to salinization separately for each level. The reason for this was to determine at which scale terrain features showed the greatest contribution to soil salinization.

After weighing each classified indicator for its ability to detect salinization, all weight values of the classifications were summed by spatial overlay to map areas of potential salinization. Thus

areas with many salinization indicators present would have higher potential salinization. An explanation of the calculation of the salinity potential weights of different indicators from the object-oriented rule based classification follows.

5.1.2.2 Vegetation indicator

As mentioned in Chapter 4 the Z values were exported in the level 1 classification. These Z values were used to define areas of vegetation stress within field blocks. The areas of vegetation stress would then serve as areas with high soil salinity potential. To create the threshold for defining vegetation stress, all polygons classified as BLOCK VEGETATION were selected and grouped into five quantiles according to their Z value. Figure 5.1 shows an example map of the five Z value vegetation stress levels.

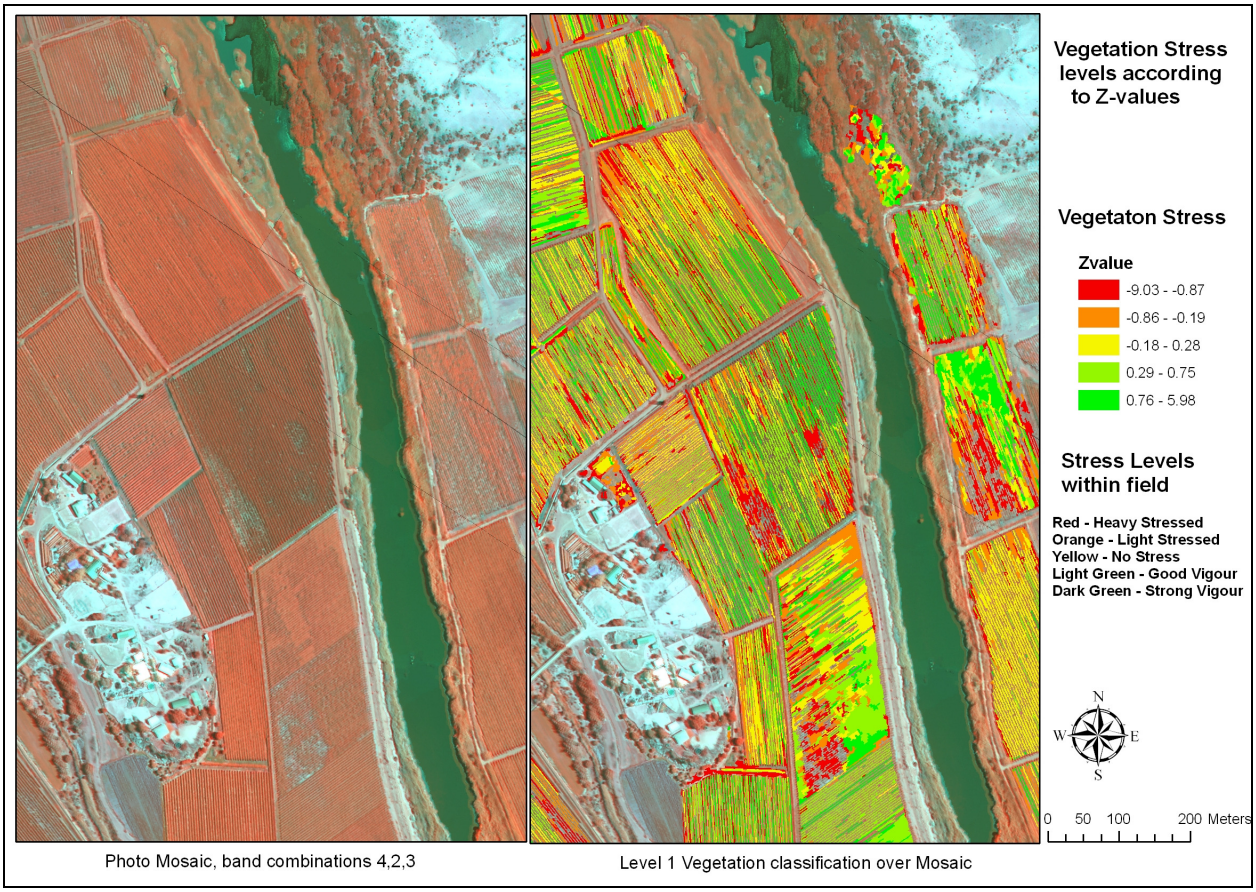

Figure 5.1. The within field vegetation stress mapped by grouping the Z values based on NDVI into five quantiles.

The high negative Z values indicate areas of vegetation growth stress. Review equation 2 in section 4.2.2.4. ($Z = (ndvi_{vegobj} - avg.ndvi_{blockveg}) / stdv.ndvi_{blockveg}$) According to equation 2, a negative Z value ($ndvi_{vegobj} - avg.ndvi_{blockveg} < 0$) indicates a vegetation object with a lower NDVI value than the average NDVI for all the vegetation objects within the field in which it is situated ($stdv.ndvi_{blockveg}$ will remain > 0). Thus negative Z values indicate a weaker vegetation index and possible vegetation stress. Therefore the 2 lower Z value quantiles will indicate a large deviation in NDVI from the average for that specific field (super object) and also indicate possible vegetation stress. The 2 higher Z value quantiles will indicate vegetation that is growing more vigorous than the average for the field.

The lowest quantile of Z values as well as the second lowest were then selected and exported as a new shapefile called "Stressed". These two classes of polygons served to indicate Heavily Stressed and Lightly Stressed vegetation. The "Stressed" shapefiles were then exported to an ESRI GRID format with 0.75m cell sizes.

5.1.2.3 Terrain indicator

In the polygon shapefile exported for each level of the terrain classification the "BestClass" field contained only two values, "unclassified" and the classified terrain feature, either a BASIN or DEPRESSION class, depending on the level. The BASIN or DEPRESSION polygons were selected in each shapefile and exported as new shapefiles of the class. These shapefiles were then exported to an ESRI GRID format at 0.75m cell resolution.

5.1.2.4 Buffering

Buffers were created for all salinized soil samples as one buffer group and all non-salinized soil samples as the other buffer group for each Analysis Block. The buffers were created at four different radii in each buffer group. Figure 5.2 shows an example of some saline and non-saline soil samples that are buffered and overlain with the classified salinity indicators.

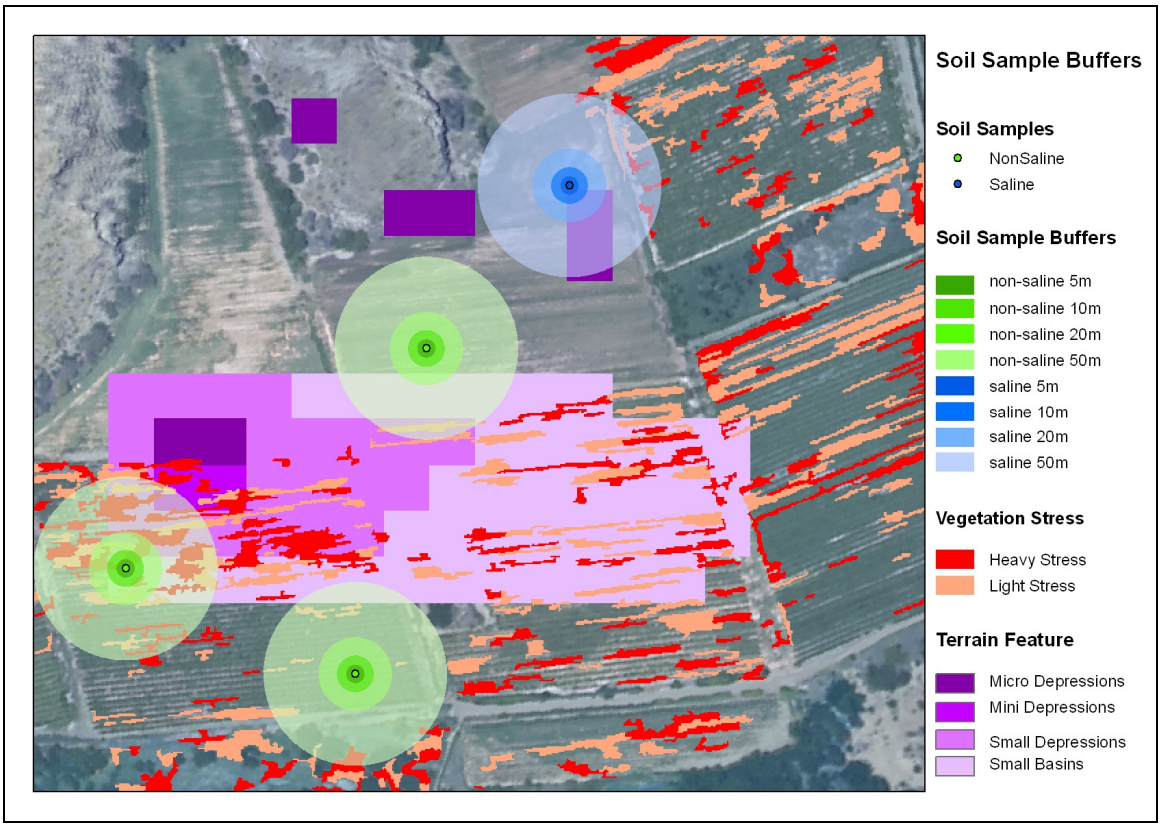

Figure 5.2. Buffered zones around soil sample locations and classified salinity indicators.

Each buffer group (saline and non-saline samples) for each Analysis Block had buffer polygons created at 5m, 10m 20m and 50m radius around the soil sample. The buffers were converted to ESRI GRID files with 0.75m cells and were used in overlays with the classified salinity indicator GRID files. The goal was to determine to what extent the salinity classes occurred within the various proximity zones around the soil samples. The reason for the different proximity zones was to accommodate the different spatial resolutions of the data used in the classifications. The DEM's were based on 25m pixel sizes whereas the photo mosaics had 0.75m pixel sizes. Analyzing at different proximity to the samples was an attempt to compensate for the differences in segmentation scale.

5.1.2.5 Calibration of salinity potential per indicator

The GRID buffers at all radii for salinized and non-salinized soil samples for each Analysis Block were used in overlay operations in ArcGis Spatial Analyst on each of the GRID file salinization indicators. The overlay operation clipped the GRID salinization indicators to within

the extent of the buffers of the soil samples (within a certain proximity to the soil samples). Thus the spatial proximity and extent of the classifications to areas of verified salinization or no salinization was determined. Figure 5.3 is an example of the vegetation indicator clipped by the 50m buffer.

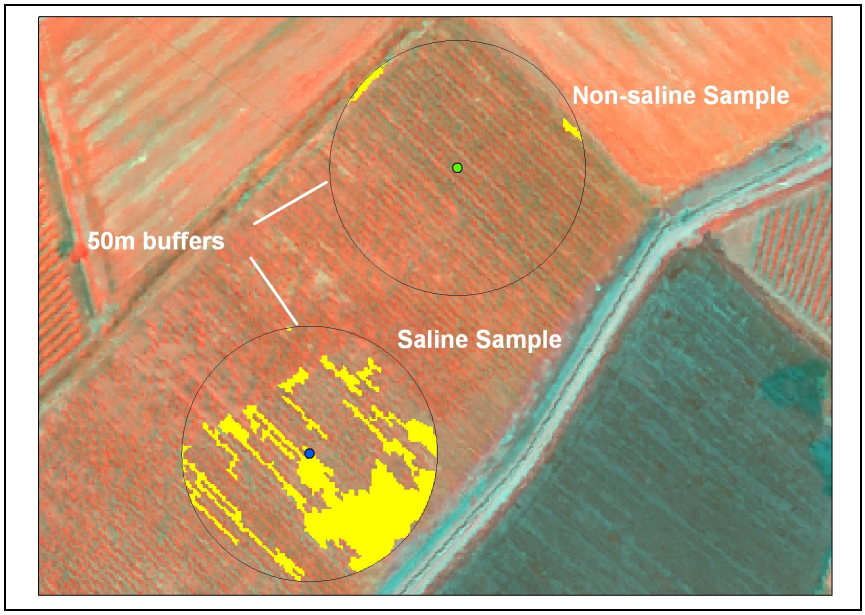

Figure 5.3. The vegetation indicator GRID file clipped with a 50m buffer around a saline and non-saline soil sample.

Because the salinity indicators were clipped GRID files, the area they covered in the four proximity zones ranging from 5m to 50m from the soil samples could also be calculated by counting the number of pixels in the proximity zone belonging to each indicator. By counting these pixels occurring within the salinized and non-salinized buffer areas for each Analysis Block, each indicator's individual frequency of occurrence around salinized and non-salinized samples indicated its correlation with high salinity.

Table 5.1 and Table 5.2 show the numbers of pixels of each indicator occurring around either saline or non-saline samples respectively for the four radii for each Analysis Block. The large scale terrain classes MEDIUM BASINS and LARGE BASINS were not found in close proximity (within any sample buffer) of any of the salinized soil samples and were therefore excluded as a salinity potential indicator from further analysis.

Table 5.1. The GRID format classifications clipped by the salinized sample buffers

Salinized									
buffer size and Analysis Block	**total pixels in sample area**	**total pixels light stress**	**total pixels heavy stress**	**total pixels micro dep**	**total pixels mini dep**	**total pixels small dep**	**total pixels small basins**	**total pixels salinity indicators**	**sum of potential in all areas**
5m									
Analysis Block 1	141	50	0	0	0	0	0	50	0.35
Analysis Block 2	416	56	45	0	0	0	0	101	0.24
Analysis Block 3	422	58	9	25	0	0	0	92	0.22
Analysis Block 4	141	0	0	0	0	0	0	0	0.00
Analysis Block 5	698	107	0	0	0	0	277	384	0.55
Analysis Block 6	416	0	0	0	0	137	137	274	0.66
All	2234	271	54	25	0	137	414	901	0.40
prop area		0.12	0.02	0.01	0.00	0.06	0.19		
prop sal		0.30	0.06	0.03	0.00	0.15	0.46		
10m									
Analysis Block 1	559	141	0	0	0	0	0	141	0.25
Analysis Block 2	1683	121	270	0	0	0	0	391	0.23
Analysis Block 3	1678	249	46	108	0	0	0	403	0.24
Analysis Block 4	559	0	0	0	0	0	0	0	0.00
Analysis Block 5	2806	308	0	0	0	0	1121	1429	0.51
Analysis Block 6	1675	0	0	0	0	432	432	864	0.52
All	8960	819	316	108	0	432	1553	3228	0.36
prop area		0.09	0.04	0.01	0.00	0.05	0.17		
prop sal		0.25	0.10	0.03	0.00	0.13	0.48		
20m									
Analysis Block 1	2230	553	0	0	0	0	0	553	0.25
Analysis Block 2	6703	565	1335	0	0	0	0	1900	0.28
Analysis Block 3	6703	1347	411	529	0	0	0	2287	0.34
Analysis Block 4	2230	0	0	0	0	0	0	0	0.00
Analysis Block 5	11169	882	0	29	29	0	4174	5114	0.46
Analysis Block 6	6693	58	0	0	0	1346	1346	2750	0.41
All	35728	3405	1746	558	29	1346	5520	12604	0.35
prop area		0.10	0.05	0.02	0.00	0.04	0.15		
prop sal		0.27	0.14	0.04	0.00	0.11	0.44		
50m									
Analysis Block 1	13966	2287	46	0	0	0	0	2333	0.17
Analysis Block 2	40686	2533	4707	0	0	0	0	7240	0.18
Analysis Block 3	41899	5566	3052	2084	0	0	0	10702	0.26
Analysis Block 4	13966	597	509	0	0	0	0	1106	0.08
Analysis Block 5	69806	5509	0	1766	1766	0	22851	31892	0.46
Analysis Block 6	34707	292	0	0	216	7645	7645	15798	0.46
All	215030	16784	8314	3850	1982	7645	30496	69071	0.32
prop area		0.08	0.04	0.02	0.01	0.04	0.14		
prop sal		0.24	0.12	0.06	0.03	0.11	0.44		
Note: Table contains numbers of pixels and proportions									

Table 5.2. The GRID format classifications clipped by the non-salinized sample buffers

Non-salinized									
buffer size and Analysis Block	total pixels in sample area	total pixels light stress	total pixels heavy stress	total pixels micro dep	total pixels mini dep	total pixels small dep	total pixels small basins	total pixels salinity indicators	sum of potential in all areas
5m									
Analysis Block 1	141	47	0	0	0	0	0	47	0.33
Analysis Block 2	2656	308	166	0	0	0	0	474	0.18
Analysis Block 3	975	0	46	0	0	0	0	46	0.05
Analysis Block 4	1539	159	228	0	0	0	0	387	0.25
Analysis Block 5	2372	76	0	0	0	0	417	493	0.21
Analysis Block 6	3486	277	142	0	0	60	60	539	0.15
All	11169	867	582	0	0	60	477	1986	0.18
prop area		0.08	0.05	0.00	0.00	0.01	0.04		
prop sal		0.44	0.29	0.00	0.00	0.03	0.24		
10m									
Analysis Block 1	559	96	0	0	0	0	0	96	0.17
Analysis Block 2	10599	1304	730	0	0	0	0	2034	0.19
Analysis Block 3	3901	118	186	0	0	0	0	304	0.08
Analysis Block 4	6142	761	755	0	0	0	0	1516	0.25
Analysis Block 5	9498	484	36	0	0	0	1679	2199	0.23
Analysis Block 6	13964	1142	740	0	0	268	268	2418	0.17
All	44663	3905	2447	0	0	268	1947	8567	0.19
prop area		0.09	0.05	0.00	0.00	0.01	0.04		
prop sal		0.46	0.29	0.00	0.00	0.03	0.23		
20m									
Analysis Block 1	2230	162	0	0	0	0	0	162	0.07
Analysis Block 2	42435	4789	3997	0	0	0	0	8786	0.21
Analysis Block 3	15640	805	697	0	0	0	0	1502	0.10
Analysis Block 4	24565	2769	2772	0	0	0	0	5541	0.23
Analysis Block 5	37968	2064	244	0	0	0	6704	9012	0.24
Analysis Block 6	55827	5936	3854	0	14	1076	1095	11975	0.21
All	178665	16525	11564	0	14	1076	7799	36978	0.21
prop area		0.09	0.06	0.00	0.00	0.01	0.04		
prop sal		0.45	0.31	0.00	0.00	0.03	0.21		
50m									
Analysis Block 1	13966	1524	301	0	0	0	0	1825	0.13
Analysis Block 2	257057	25443	22250	0	0	0	0	47693	0.19
Analysis Block 3	94327	5769	6171	0	0	0	0	11940	0.13
Analysis Block 4	150631	16898	11908	0	0	0	0	28806	0.19
Analysis Block 5	224225	9158	1017	999	999	0	41217	53390	0.24
Analysis Block 6	333295	33069	22541	0	2245	6876	8359	0	0.22
All	1073501	91861	64188	999	3244	6876	49576	216744	0.20
prop area		0.09	0.06	0.00	0.00	0.01	0.05		
prop sal		0.42	0.30	0.00	0.01	0.03	0.23		
Note: Table contains numbers of pixels and proportions									

The “sum of potential in all areas” field shows the total number of salinity indicator pixels in the Analysis Block divided by the total number of pixels in a particular buffer distance (thus the proportion of the proximity zone containing a salinity potential indicator). The row “All” and field “sum of potential in area” shows a higher value in each buffer zone for the saline samples (Table 5.1) than the non-saline samples (Table 5.2). This means that for all proximity zones

(buffer distances) in all Analysis Blocks the average "sum of potential" was higher for salinized than non-salinized samples. Thus on average the salinized samples had more classified salinity indicator pixels in each proximity zone per Analysis Block than non-salinized samples. Thus the classifications for salinity potential indicators can be considered to be more common around true salinization than non-salinization and is therefore effective for detecting salinity. In most individual cases per Analysis Block the "sum of potential" was also higher in salinized samples than non-salinized samples.

To quantify how much more salinity indicator pixels occurred around saline than non-saline samples, the ratio of saline "sum of potential" versus the equivalent non-saline "sum of potential" was calculated for each proximity zone. In this calculation the "sum of potential" per buffer distance for saline samples were divided by the equivalent value for non-saline samples. See Table 5.3 for the ratio of "sum of potential" amounts for saline versus non-saline samples.

Table5.3. The "sum of potentials" field of the saline versus the non-saline buffers aggregated over all analysis blocks.

Buffer distance	Total of potentials in salinized areas	Total of potentials in non-salinized areas	Ratio of salinized to non-salinized
5m	0.403	0.178	2.268
10m	0.360	0.192	1.878
20m	0.353	0.207	1.704
50m	0.321	0.202	1.591

According to Table 5.3 the extent of potential salinity was more than twice as frequent around the closest proximity zone, but becoming increasingly less with an increase of the proximity zone around the samples. The extent of potential salinity was on average at least 59% more around saline samples than non-saline samples (from the 50m buffer). Thus classified salinity potential in the study was most accurate at the closest proximity to the sample, and therefore future studies using this research methodology should preferably use high spatial resolution data (<5m) to detect potential salinization.

The next step was to determine which indicators were the most important in determining salinity potential for the purpose of assigning them a salinity potential weight. This weight was used for

the creation of salinity potential maps. The important entries for this purpose in Tables 5.1 and 5.2 are the last two rows below each buffer size ("prop area" and "prop sal").

The values in the row "prop area" shows the proportion of the area that the specific indicator occupies. Equation (3) illustrates how it was calculated:

$$P_{af(ij)} = f_i/b_j \qquad (3)$$

Where $P_{af(ij)}$ was the proportion of the area occupied by the indicator f_i with i being the specific indicator (eg. Light Stressed). Further, f_i was the total number of pixels over all Analysis Blocks for the indicator i in the buffer size j. The buffer is shown by b_j with j the buffer size (eg. 5m) and b_j the total pixels in buffer size j over all Analysis Blocks (row "All", column "total pixels in sample area").

The "prop sal" entry expresses the total area of a specific stress indicator as a proportion of the total area occupied by all the stress indicators and thus gives the salinity potential weight for that specific stress indicator per buffer zone. Equation (4) illustrates how it was calculated:

$$P_{s(ij)} = P_{af(ij)}/\Omega \qquad (4)$$

Where $P_{s(ij)}$ was the proportion that indicator i contributes in buffer size j to salinity from all the indicators. $P_{af(ij)}$ is defined in equation (3). Furthermore, Ω was defined as $\Sigma f_n/b_j$. Σf_n indicates the sum of salinity indicator pixels in buffer size j and n being the set of all salinity indicators (row "All", column "sum of potential in area"). b_j is defined as in (3), the total number of buffer pixels for buffer size j . Thus $\Sigma P_{s(ij)}$ for $n = 1$.

The calibration for potential weights was taken a step further by summing the occurrence of each stress indicator over all buffers and then averaging the "prop area" ($avg(P_{af(ij)})$) values for each indicator. Table 5.4 illustrates the next steps.

Table 5.4. The calculation of the salinity potential weights for each indicator based on Tables 5.1 & 5.2.

Calculation step	Light Stressed	Heavy Stressed	Micro Dep	Mini Dep	Small Dep	Small Basins	Total Potential
saline.avg($P_{af(ij)}$)	0.097	0.037	0.014	0.003	0.046	0.164	0.323
non-saline.avg($P_{af(ij)}$)	0.086	0.058	0.000	0.001	0.006	0.044	
R_{sns}	1.125	0.635	61.000	3.235	7.679	3.719	
saline.avg($P_{af(ij)}$)*R_{sns}	0.109		0.866	0.008	0.351	0.609	1.942
potential weight	0.056		0.446	0.004	0.181	0.314	1.000
final weight rounded	**0.06**		**0.45**		**0.18**	**0.31**	**1**

This value in the saline buffers (saline.avg($P_{af(ij)}$)) was then divided by that of the non-saline buffers (non-saline.avg($P_{af(ij)}$)) to get the measure of difference between the presence of the indicator in saline and non-saline areas, expressed as a ratio (R_{sns}). Ratios less than 0 indicated that the indicator was more common in non-saline buffers and was therefore discarded, as was the case for the "Heavy Stress" indicator. The reasons why "Heavy Stress" was not an indicator of salinization could be manifold. Stony, sandy or waterlogged soils were given as reasons for vegetation stress other than high salinity by the field teams that collected the soil samples (Volschenk et al. 2005).

The potential value (saline.avg($P_{af(ij)}$)*R_{sns}) for each indicator was calculated as the average of the "prop area" values (saline.avg($P_{af(ij)}$)) for all buffer sizes multiplied by the saline non-saline ratio (R_{sns}). This potential value is thus the extent of an indicator occurring in saline buffers (saline.avg($P_{af(ij)}$)) combined with its seperability from the extent of occurrence in non-saline buffers (R_{sns}). The potential value was then divided by the total of potential values (last column in Table 5.4) for all indicators to get the final salinity potential weight of the indicator.

The results of the salinity weight calculation showed that MICRO DEPRESSIONS carried the highest salinity potential and Light Stressed vegetation the lowest. Once again vegetation stress could not be considered as a good indicator of salinity in this context as other factors may also induce plant stress. The field teams reported that high salinity, causing vegetation stress, was found mostly at the lowest elevation points in the floodplain (Volschenk et al. 2005). Thus the derived potential weight indicating the importance of terrain indicators is affirmed.

5.2 CREATION OF SALINITY POTENTIAL MAPS

The next step was to create maps of salinity potential in all the Analysis Blocks using the classifications and the potential weights derived for the different indicators. The spatial data for the maps were of the same format (0.75m GRID) as the data for deriving salinity potential weights. The shapefiles from the raw classifications were edited by adding a new field with the weight of salinity potential. The shapefiles were then converted to ESRI GRID files with 0.75m cell sizes using the weight field as cell value. The GRID files for each indicator were then overlain and the potential values added together in Spatial Analyst.

Large scale terrain indicator classes such as SMALL BASINS were often located on the river. This is due to the river course often being the lowest elevation point in an area and water thus draining towards this point. The classification as an area of entrapped or very little drainage outwards is thus incorrect. Therefore the classified WATER class was used to mask out the salinity potential GRID pixels wherever it was located on the river.

The salinity potential indicators were assumed to be additive. Regions with more than one salinity indicator had the salinity potential of the sum of all the indicators present. Figures 5.4 – 5.9 show the final salinity potential maps for analysis blocks 1- 6 respectively.

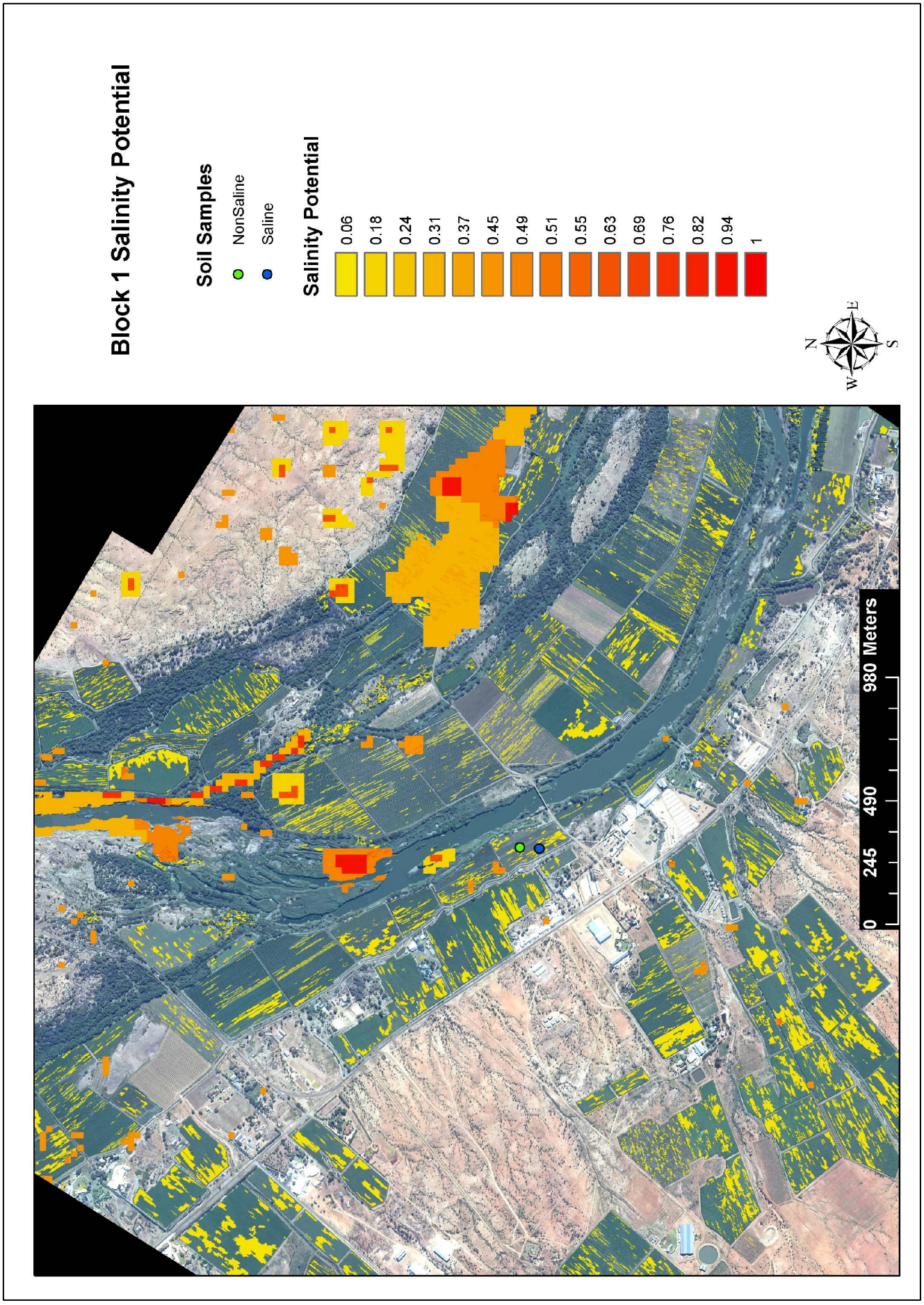

Figure 5.4. Salinity potential map for Analysis Block 1

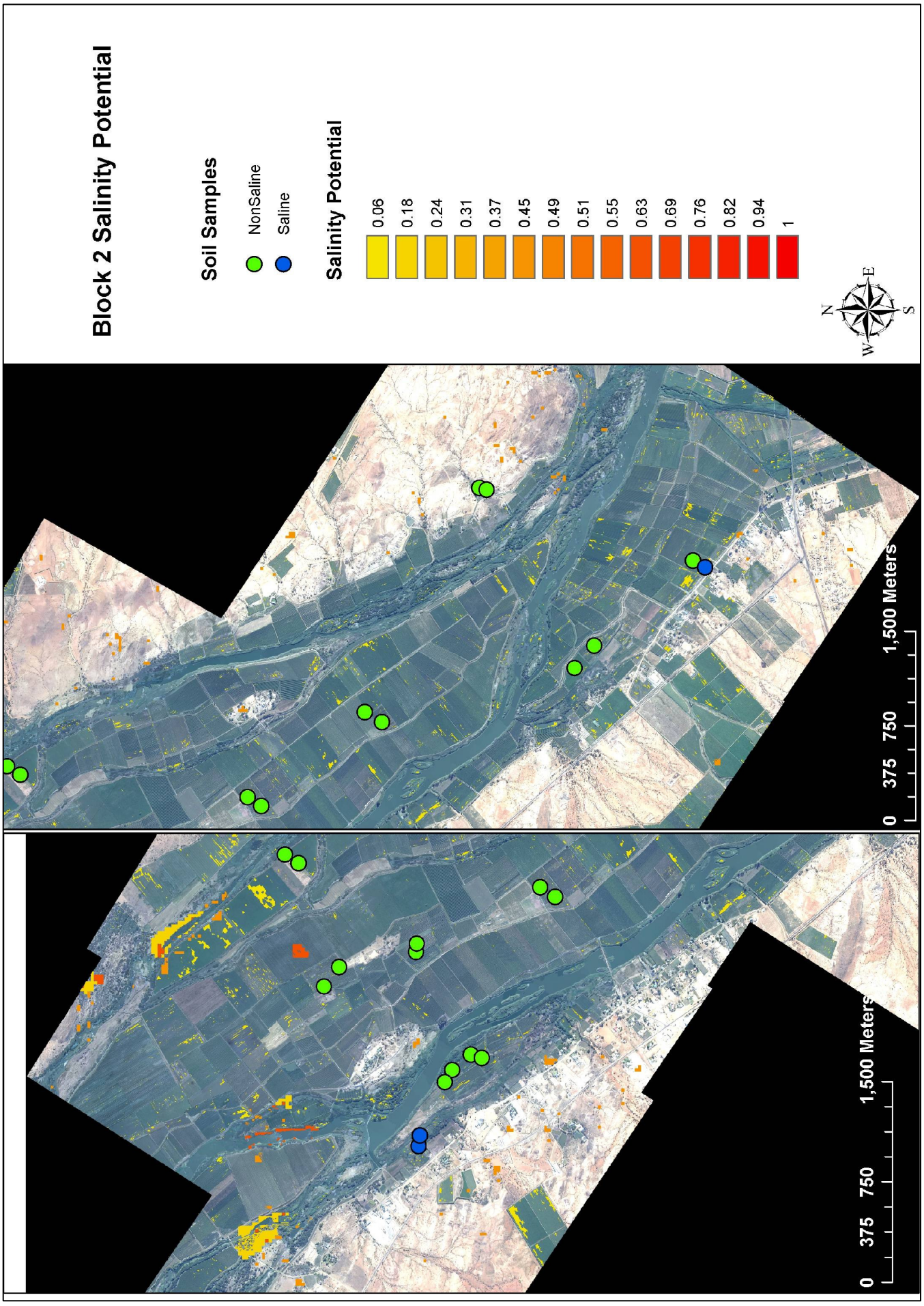

Figure 5.5. Salinity potential map for Analysis Block 2

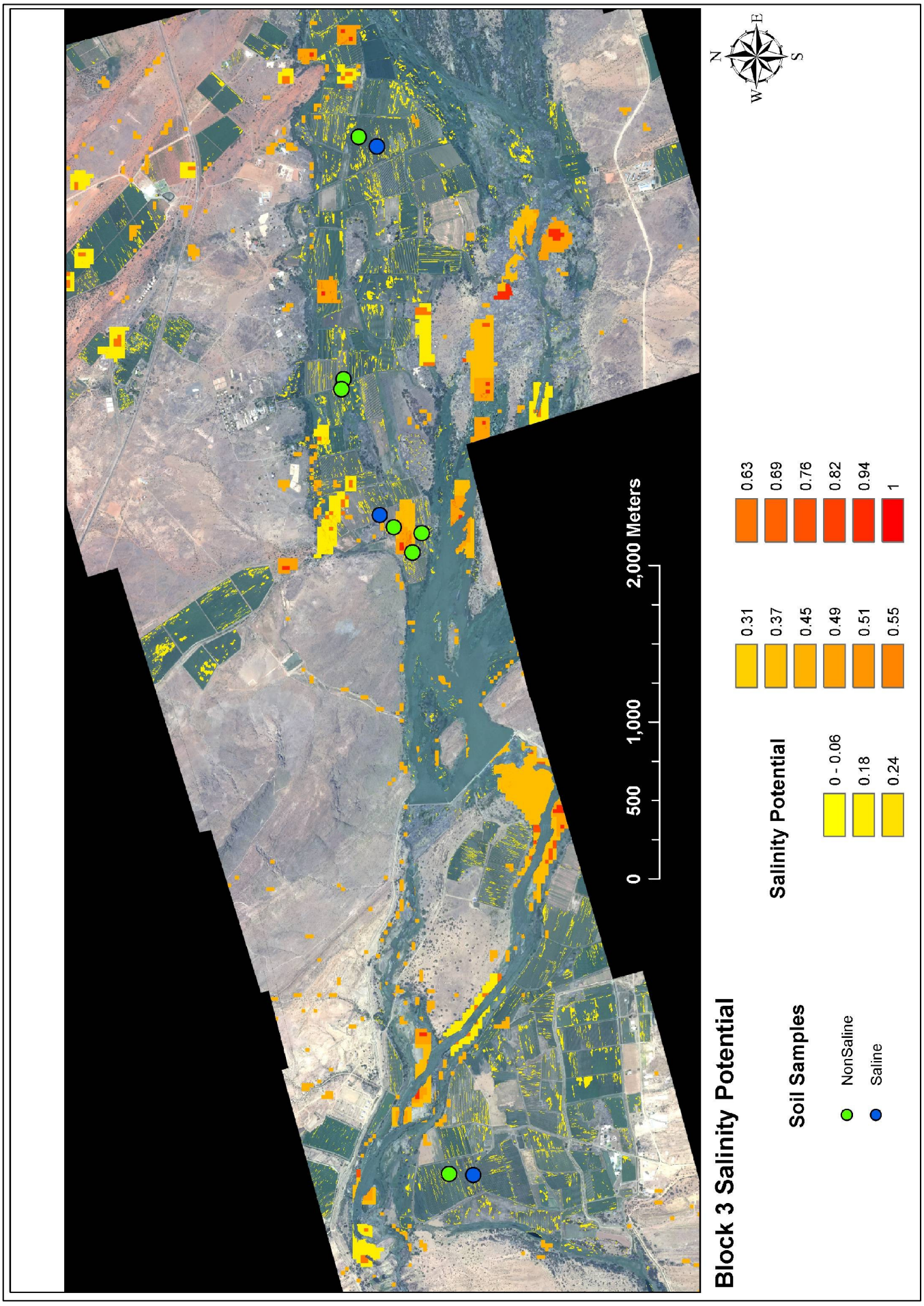

Figure 5.6. Salinity potential map for Analysis Block 3

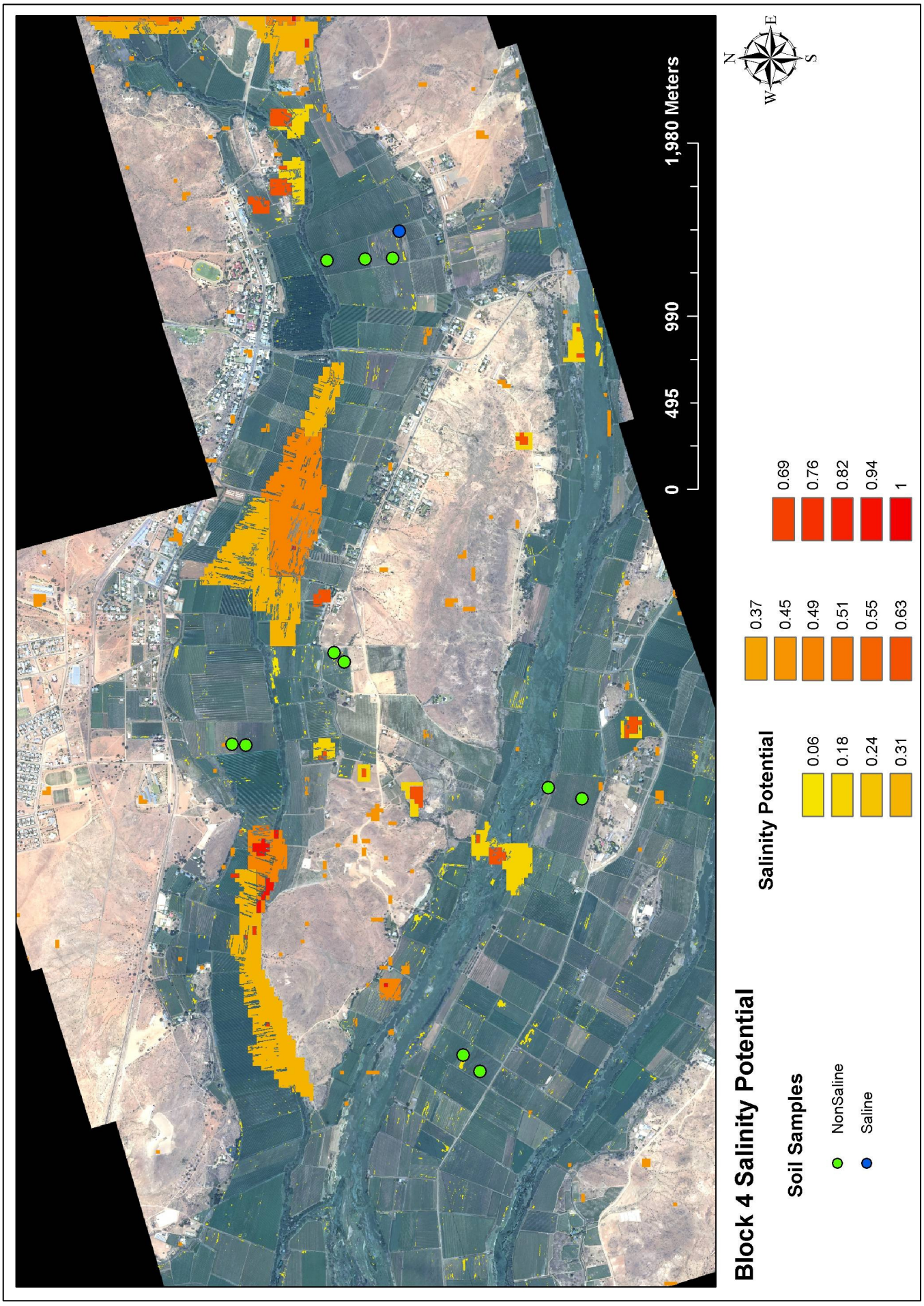

Figure 5.7. Salinity potential map for Analysis Block 4

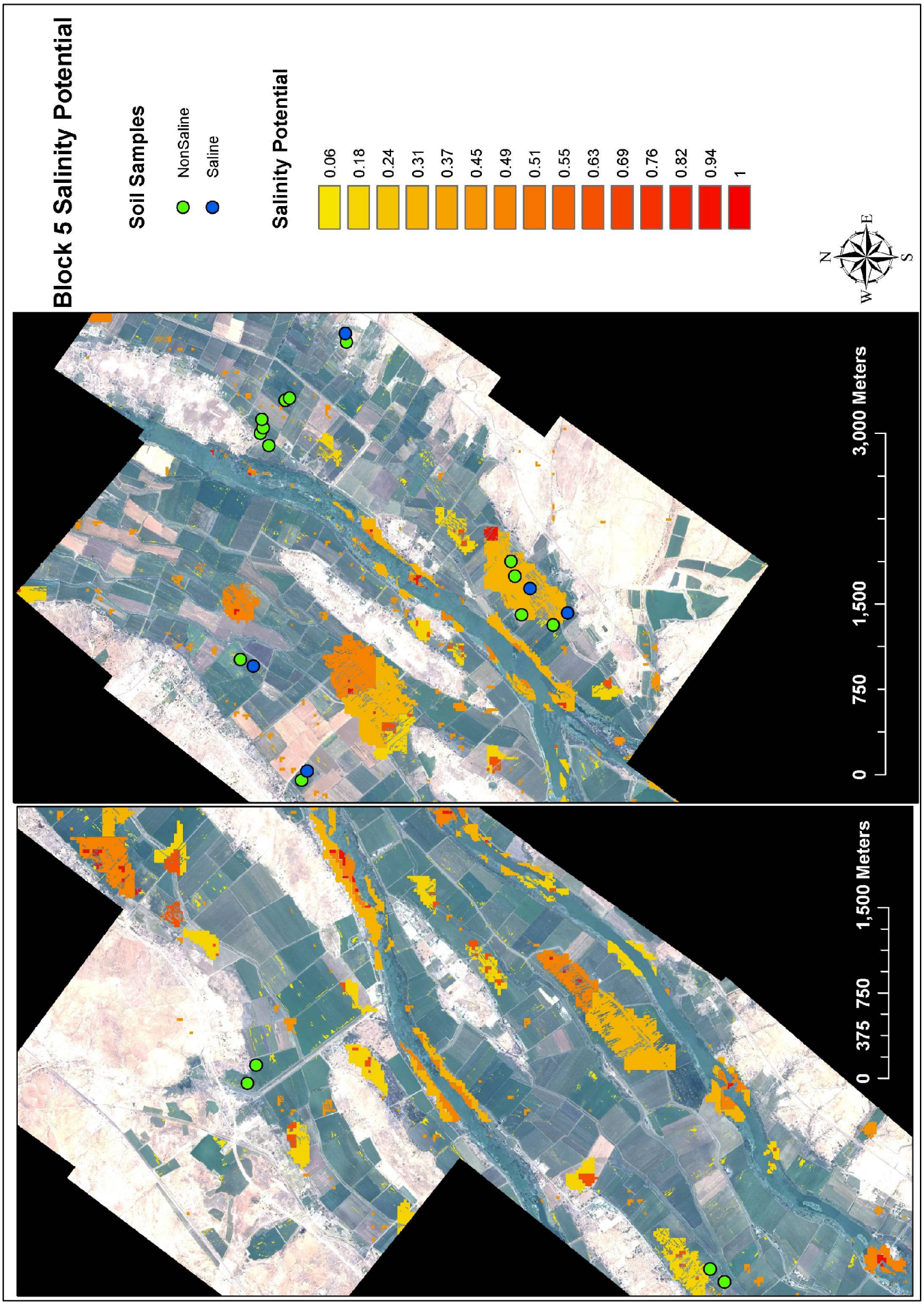

Figure 5.8. Salinity potential map for Analysis Block 5

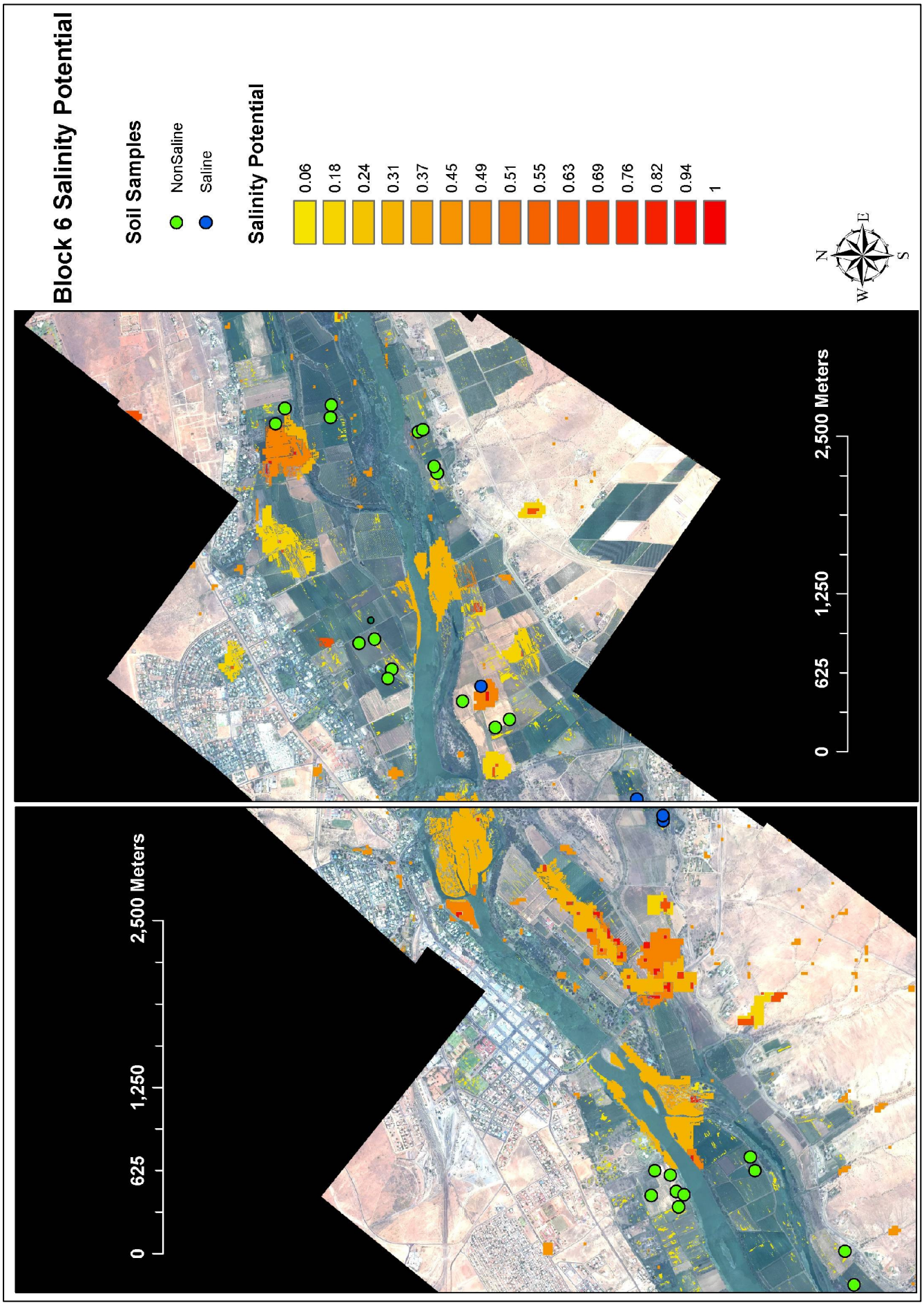

Figure 5.9. Salinity potential map for Analysis Block 6

This chapter discussed the creation of salinity potential weights for the different high salinity indicators derived from the object-oriented classification of the photo images and DEM's as well as how these potentials were used to create salinity potential maps. These maps can not be tested for accuracy in indicating true salinity using the available soil sample data, because the data was already used to calibrate the potential weights for the indicators. The maps can however be of value in the collection of new soil samples by guiding the field workers to areas of high potential salinity. The next chapter is a final discussion and summary of the entire research.

6: DISCUSSION AND SUMMARY

The aim of the research was to ascertain whether object-oriented image analysis could be used to identify and map areas of potential soil salinization. These areas were identified by creating rule based classification procedures which could be applied to radiometrically calibrated digital aerial photograph mosaics as well as to DEM's. The classification products were used to create potential soil salinity maps based on different classifications having different salinity potentials.

6.1 VEGETATION IMAGE ANALYSIS

The rule base for spectral classification of vegetation in colour infrared (CIR) showed good classification accuracies. Individual crop fields could be classified by a combination of edge detection added to the image data and the segmentation capabilities offered by the software. Although the classification stability was not very good at the higher hierarchical field level (3), the accuracy test by confusion matrix showed good accuracy at level 2. The stability weakness could be ascribed to the way the classification rules were utilized at different hierarchical levels of objects.

The vegetation classes could be identified to a very fine spatial resolution up to the level of individual crop rows. The vegetation classification at this fine level could also be separated from within bare soils rows by utilizing the fuzzy classification capability and different rules based on expert knowledge. Mixed pixels, fine spatial scale and considerable variability of vegetation appearance within a field would have made a purely spectral based classification unsuccessful.

The rule based expert knowledge classification was successful for separation of small objects into different classes. The classification stability and best classification result for level 1 was indicative of a good, stable definition of rules for identifying within field vegetation features such as vineyard rows.

The capability of object-oriented classification to create GIS ready products was illustrated by the calculation of the Z value using customized features for the within field objects during the classification stage. Thus the classification result could be exported and the Z value used for determining stress level directly in the GIS without any need to set up further statistics. The ability to create these customized features which conduct exportable, GIS ready calculation results during classification is a powerful tool which could be used in future applications.

6.2 TERRAIN IMAGE ANALYSIS

Unfortunately the accuracy of real world terrain features identified on the DEM could not be tested as no reference data for terrain units were available. The software did make identifying these features simple by rule definitions based on the object features. Terrain features could also be identified at different spatial scales in the object hierarchy in one classification step. The ability of object-oriented software to define terrain units such as basins and depressions by utilizing the features of segmented objects is a topic for further research.

6.3 SALINITY DETECTION

The classifications of potential areas of high salinity by object-oriented methods had some success in identifying actual salinity. On average stressed vegetation based on NDVI values was not a good indicator of potential salinity. Although the amount of land with lightly stressed vegetation found around saline samples exceeded the area covered by terrain indicators (from Table 5.1), the non-salinized samples had nearly as much land covered by light vegetation stress and even more by heavy vegetation stress (compare Tables 5.1 & 5.2). Terrain indicators at the micro depression scale as well as small basins were on average much more abundant around saline samples and thus served as better indicators of actual salinity. This difficulty in distinguishing actual saline soil from non-saline areas by the classified indicators, emphasizes the complexity and constraints that exist in detecting salinization by remote sensing. The higher correlation between salinity and terrain indicators than vegetation indicators requires further

investigation of the terrain indicator in further studies. Topography may potentially hold more promise for detecting salinity in irrigated agriculture than vegetation stress.

6.4 IMPROVEMENTS AND RECOMMENDATIONS

Several shortcomings of the study have been identified. Insufficient accuracy of the orthorectified digital aerial images could have degraded the spectral reliability of the image mosaics. The lack of a camera calibration report resulted in lower accuracy of the interior and exterior camera orientation parameters. This affected the spatial accuracy and matching of the NIR photos on the RGB photos and the matching of photo overlays during the mosaicking phase. Although the rectified photos appeared satisfactory, some areas with errors were still noted. These spatial mismatches would have negatively affected the spectral integrity of the mosaics and thus the vegetation indices.

In the vegetation stress classification, the classification of large open soil patches in fields could also serve as salinity and stress indicators. Such a classification was attempted, but was extremely difficult at the finest spatial resolution. This class could not be defined satisfactorily due to time constraints on the project.

The lack of the calibration report and sufficiently accurate internal and external orientation parameters meant that Digital Terrain Models (DTM's) could not be created in the orthorectification process. If this had been possible DTM's would have been available with better spatial resolution than the 25m DEM's that were used. A higher resolution DEM would have reduced the mismatch in scale of analysis between the photo mosaics (0.75m) and the terrain indicators. Further studies using these image analysis methods should use terrain data of finer spatial resolution. Finer resolution terrain data could potentially deliver more valuable results.

The number of soil samples used for analysis should be increased, especially the salinized samples. Too few salinized soil samples were available to calibrate the classifications of salinity indicators to assign salinity potential weights and to test the salinity potential maps against other

soil samples not used in calibration. The accuracy of the salinity potential maps could not be tested effectively without more soil samples, especially saline samples.

6.5 SUMMARY

Object-oriented image analysis offers a powerful way to classify fine detail classes in high resolution data. The features available in the objects derived from image segmentation provide ways for detailed classification of high resolution vegetation image data, identifying terrain features and complex statistical calculations as GIS ready information. These classifications and object segmentations can be conducted at different spatial scales within a hierarchy of levels, offering context and relationship information within and between levels, objects and classes. This, in conjunction with the rule based fuzzy classification capability, offers tools for complex classification definitions. The use of expert knowledge in classification could be incorporated within this framework. Object-oriented image analysis can thus be used as a tool in monitoring environmental phenomena such as salinity potential. Spatially and spectrally accurate data at this high resolution level is a prerequisite for good results though. The rule bases have been set up on a calibration area and applied successfully for automated classification of other areas using the protocol functionality.

REFERENCES

Alexandratos, N (ed.) 1995. *World Agriculture: Towards 2010.* FAO, Rome and Wiley, Chichester.

Argialas D & Tzotsos A 2006. Automatic extraction of physiographic features and alluvial fans in Nevada, USA from digital elevation models and satellite imagery through multiresolution segmentation and object-oriented classification. ASPRS Annual Conference, Reno, Nevada: May 1-5.

Baatz M, Benz U, Dehghani S, Heynen M, Höltje A, Hofmann P, Lingenfelder I, Mimler M, Sohlbach M, Weber M & Willhauck G 2004. eCognition Professional User Guide 4. München: Definiens Imaging GmbH.

Barrow CJ 1991. *Land Degradation. Development and Breakdown of Terrestrial Environments.* Cambridge: Cambridge University Press.

Bauer T & Steinnocher K 2001. Per-parcel land use classification in urban areas applying a rule-based technique. *GIS – Zeitschrift für Geoinformationssysteme* 6:24-27.

Bear FE 1955 (ed.) *Chemistry of the soil*. New York : Reinhold.

Benz UC, Hofmann E, Willhauck G, Lingenfelder I & Heynen M 2006. Multi-resolution, object-oriented fuzzy analysis of remote sensing data for GIS-ready information. *Photogrammetry & Remote Sensing* 58: 239-258.

Blaschke T & Strobl J 2003. Defining Landscape Units Through Integrated Morphometric Characteristics. [online] available at: http://www.definiens.com/documents/publications_earth2003.php [Accessed 9 August 2006].

Blaschke T & Strobl J 2001. What's wrong with pixels? Some recent developments interfacing remote sensing and GIS. *GIS – Zeitschrift für Geoinformationssysteme* 6:12-17.

Bresler E, McNeal BL and Carter DL 1982. *Saline and Sodic Soils. Principles-Dynamics-Modeling.* Berlin : Springer-Verlag.

Brooks CN, Schaub DL, Powell RB, French NHF & Shuchman RA 2006. Multi-Temporal and Multi-Platform Agricultural Land Cover Classification in Southeastern Michigan. ASPRS Annual Conference, Reno, Nevada: May 1-5.

Burnett C & Blaschke T 2003. A multi-scale segmentation/object relationship modelling methodology for landscape analysis. *Ecological Modelling* 168: 233-249.

Campbell JB 2002. *Introduction to Remote Sensing.* 3rd ed. London: Taylor and Francis Ltd.

Chen L, Chiang T & Teo T 2005 Fusion of LIDAR Data and High Resolution Images for Forest Canopy Modeling. [online] available at: http://www.definiens.com/documents/publications_earth2005.php [Accessed 9 August 2006]

Darwish T, Atallah T, El Moujabber M & Khatib N 2005. Salinity evolution and crop response to secondary soil salinity in two agro-climatic zones in Lebanon. *Agricultural Water Management* 78: 152-164.

Dehaan RL & Taylor GR 2002. Field-derived spectra of salinized soils and vegetation as indicators of irrigation-induced soil salinization. *Remote Sensing of Environment* 80: 406-417.

Douaoui AEK, Nicolas H & Walter C 2005 (in press). Detecting salinity hazards within a semiarid context by means of combining soil and remote-sensing data. *Geoderma.*

Dwivedi RS & Sreenivas K 2002. The vegetation and waterlogging dynamics as derived from spaceborne multispectral and multitemporal data. *International Journal of Remote Sensing* 23(14):2729-2740

Dwivedi RS, Sreenivas K & Ramana KV 1999. Inventory of salt-affected soils and waterlogged areas: a remote sensing approach. *International Journal of Remote Sensing* 20(8):1589-1599.

Eldiery A, Garcia LA & Reich RM 2005. Estimating Soil Salinity from Remote Sensing Data in Corn Fields. Hydrology Days, 26th Annual American Geophysical Union [online] available at: http://www.hydrologydays.colostate.edu/Papers_2005/Ahmed_paper.pdf [Accessed 9 August 2006].

Ghassemi F, Jakeman AJ & Nix HA 1995. Salinization of land and water resources: human causes, extent, management and case studies. Canberra, Australia: The Australian National University, Wallingford, Oxon, UK: CAB International.

Gibson PJ, Power CH & Keating J 2000. *Introductory Remote Sensing: Principles and Concepts.* London: Routledge.

Golovina NN, Minskiy D, Pankova Y & Soloyev DA 1992. Automated air photo interpretation in the mapping of soil salinization in cotton-growing zones. *Mapping sciences and Remote Sensing* 29:262-268.

Hoffman T 1998. *Orange River Nama Karoo*. [online]. Pretoria: Department of Environmental Affairs and Tourism. Available from http://www.ngo.grida.no/soesa/nsoer/Data/vegrsa/veg51.htm [Accessed 11 January 2007]

Hoffmann A & Van der Vegt JW 2001. New Sensor systems and new Classification Methods: Laser- and Digital Camera-data meet object-oriented strategies. *GIS – Zeitschrift für Geoinformationssysteme* 6:18-23.

Horney RD, Taylor B, Munk DS, Roberts BA, Lesch SC & Plant RE 2005. Development of practical site-specific management methods for reclaiming salt affected soil. *Computers and electronics in agriculture* 46:379-397.

Johnson LF, Roczen DE, Youkana SK, Nemani RR & Bosch DF 2003. Mapping vineyard leaf area with multispectral satellite imagery. *Computers and electronics in agriculture* 38:33-44.

Kirkby SD 1996. Integrating a GIS with an expert system to identify and manage dryland salinization. *Applied Geography* 14(4):289-303.

Khan NM, Rastoskuev VV, Sato Y & Shiozawa S 2005. Assessment of hydrosaline land degradation by using a simple approach of remote sensing indicators. *Agricultural Water Management* 77:96-109.

Lobo A, Chic O & Casterad A 1996. Classification of Mediterranean crops with multisensor data: per-pixel versus per-object statistics and image segmentation. *International Journal of Remote Sensing* 17(12):2385-2400.

Mashimbye ZE 2004. Remote Sensing-based identification and mapping of salinized irrigated land between Upington and Keimoes along the Lower Orange River, South Africa. MSc-thesis. Stellenbosch: University of Stellenbosch, Department of Geography and Environmental Studies.

McFarlane DJ & Williamson DR 2002. An overview of water logging and salinity in southwestern Australia as related to the 'Ucarro' experimental catchment. *Agricultural Water Management* 53:5-29.

Metternicht GI 2001. Assessing temporal and spatial changes of salinity using fuzzy logic, remote sensing and GIS. Foundations of an expert system. *Ecological Modelling* 144:163-179.

Metternicht GI & Zinck JA 1996. Modelling salinity-alkalinity classes for mapping salt-affected topsoils in the semi-arid valleys of Cochabamba (Bolivia). *ITC Journal 1996* 2:125-135.

Metternicht GI & Zinck JA 1997. Spatial discrimination of salt- and sodium affected soil surfaces. *International Journal of Remote Sensing* 18:2571-2586.

Metternicht GI & Zinck JA 2003. Remote sensing of soil salinity: potentials and constraints. *Remote Sensing of Environment* 85:1-20.

Moolman JH, De Clerq WP, Wessels WPJ, Meiri A & Moolman CG 1999. The use of saline water for irrigation of grapevines and the development of crop salt tolerance indices. (Report No. 303/1/98) Pretoria: Water Research Commission.

Mougenot B, Pouget M & Epema G 1993. Remote sensing of salt-affected soils. *Remote Sensing Reviews* 7:241-259.

Oruc M, Marangoz AM & Buyuksalih G 2004. Comparison of pixel-based and object-oriented classification approaches using Landsat-7 ETM spectral bands. [online] available at: http://www.definiens.com/documents/publications_earth2004.php [Accessed 9 August 2006].

Pannel DJ & Ewing MA 2006. Managing secondary dryland salinity: Options and challenges. *Agricultural Water Management* 80:41-56.

Peck AJ & Hatton T 2003. Salinity and the discharge of salts from catchments in Australia. *Journal of Hydrology* 272:191-202.

Pinter PJ, Hatfield JL, Schepers JS, Barnes EM, Moran MS, Daughtry CST & Upchurch DR 2003. Remote Sensing for Crop Management. *Photogrammetric Engineering & Remote Sensing* 69(6):647-664.

Rego LFG & Koch B 2003. Automatic classification of land cover with high resolution data of the Rio De Janeiro City Brazil. Comparison between pixel and object classification. [online] available at: http://www.definiens.com/documents/publications_earth2003.php [Accessed 9 August 2006].

Rezaei SA & Gilkes RJ 2005. The effects of landscape attributes and plant community on soil chemical properties in rangelands. *Geoderma* 125:167-176.

Sah A, Apisit E, Murai S &Parkpian E 1995. Mapping of salt-affected soils using remote sensing and geographic information systems: a case study of Nakhon Ratchasima, Thailand. *Proceedings of the 16th Asian Conference Remote Sensing 20-24 November* (pp. G-3-1 – G-3-6). Thailand: Nakhon Ratchasima.

Schiewe J, Tufte L & Ehlers M 2001. Potential and problems of multi–scale segmentation methods in remote sensing. *GIS – Zeitschrift für Geoinformationssysteme* 6:34-39.

Schiewe J 2002. Segmentation of high-resolution remotely sensed data – concepts, applications and problems. In Joint Symposium on Geospatial Theory, Processing and Applications Ottawa, Canada [online] available at: http://www.definiens.com/documents/publications_earth2002.php [Accessed 9 August 2006].

Steila D 1976. *The Geography of Soils. Formation, distribution and management*. New Jersey : Prentice-Hall.

Stocking 1995. Soil erosion and land degradation. In O'Riordan T (ed) *Environmental Science for Environmental Management*, pp223-242. Harlow: Longman.

Szabolcs I 1998. Salt Buildup as a Factor of Soil Degradation. In Lal R, Blum WH, Valentine C & Stewart BA (eds.) *Methods for Assessment of Soil Degradation,* pp253-264. New York: CRC Press.

Thorne DW & Seatz LF 1955. Acid, Alkaline, Alkali and Saline Soils. In Bear FE (ed) *Chemistry of the soil,* pp219-252. New York: Reinhold.

Tooth S & McCarthy TS 2004. Anabranching in mixed bedrock alluvial rivers: the example of the Orange River above Augrabies Falls, Northern Cape Province, South Africa. *Geomorphology* 57:235-262.

Tuominen S & Pekkarinen A 2004. Local radiometric correction of digital aerial photographs for multi source forest inventory. *Remote Sensing of Environment* 89:72-82.

University of Manitoba 2006. Natural Resources Institute [online] available at: http://www.umanitoba.ca/institutes/natural_resources/gallery/canada/manitoba_prairies/smmanitobaprairies3.jpg [Accessed 11 November 2006].

US Salinity Laboratory 1954. *Diagnosis and improvement of saline and alkali soils.* Washington D.C.: United States Department of Agriculture.

Utset A & Borroto M 2001. A modelling-GIS approach for assessing irrigation effects on soil salinization under global warming conditions. *Agricultural Water Management* 50:53-63.

Volschenk T, Fey M & Zietsman HL 2005. Situation analysis of problems for water quality management in the Lower Orange River region (with special reference to the contribution of the foothills to salinization). (Report No. 1358/1/05). Stellenbosch: Agricultural Research Council.

Wang D, Wilson C, Shannon MC 2002. Interpretation of salinity and irrigation effects on soybean canopy reflectance in visible and near-infrared spectrum domain. *International Journal of Remote Sensing* 23(5):811-824.

Water Research Commission 1999. Evaporation from the Orange River: quantifying open water resources. (Report No. 683/1/99), Pretoria: Water Research Commission.

Wells G & Holz RK 1985. Photography beyond the Red. In Holz RK (ed) *The surveillant science,* pp185-195. New York: John Wiley & Sons Inc.

Whiteside T & Ahmad W 2004. A comparison of object-oriented and pixel-based classification methods for mapping land cover in Northern Australia. In Proceedings of SSC2005 Spatial intelligence, innovation and praxis: The biennial Conference of the Spatial Sciences Institute Melbourne, Australia available at: http://www.definiens.com/documents/publications_earth2004.php [accessed 9 August 2006].

Wild A 2003. *Soils, land and food*. Cambridge University Press.

Willhauck G 2000. Comparison of object oriented classification techniques and standard image analysis for use of change detection between SPOT multispectral satellite images and aerial photos. ISPRS, Vol. XXXIII, Amsterdam

Yuan F & Bauer ME 2006. Mapping impervious surface area using high resolution imagery: a comparison of object-based and per-pixel classification. ASPRS Annual Conference, Nevada: May 1-5.

Zevenbergen LW & Thorne CR 1987. Quantitative analysis of land surface topography. *Earth Surface Processes and Landforms* 12: 47-56.

Zhang Y & Maxwell T 2006. A fuzzy logic approach to supervised segmentation for object-oriented classification. ASPRS Annual Conference, Nevada: May 1-5.

PERSONAL COMMUNICATIONS

Lück W 2006. Remote Sensing Researcher, Centre for Geographical Analysis, Stellenbosch University. Stellenbosch. Workshop on 27 March about object-oriented image classification.